




Cite this: DOI: 10.1039/d5cc03028e

Biomass-derived carbon quantum dots as fluorescent probes for biosensing: a review

Wen He,^{*a} Deliang Zhang,^a Yan Gao,^a Dongrun Li,^a Xing Gao,^a Hongyu Mou^{*a} and Jibin Song ^{*bc}

The conversion of biomass waste into value-added carbon quantum dots (CQDs) has been recognized as a green synthetic pathway in CQD manufacturing. The distinctive nanostructure of biomass-derived carbon quantum dots (BCQDs) confers superior fluorescence properties and biocompatibility, rendering them highly promising as fluorescent probes for biosensing applications. The preparation of BCQD fluorescent probes using biomass as the primary carbon source not only realizes the high-quality recycling of waste resources but also has excellent biocompatibility and fluorescence emission stability, which has received great attention from researchers. This review offers a comprehensive analysis of BCQDs, encompassing various carbon sources including both waste and non-waste renewable materials. It systematically examines three fundamental properties, two primary synthesis techniques, three distinct luminescence mechanisms, three sensing mechanisms, nitrogen and sulfur elemental doping strategies enhancing quantum yield (QY), as well as the most recent advancements in the biosensing applications of BCQDs. Additionally, this review identifies existing research challenges and suggests prospective directions for future investigation in this emerging domain.

Received 29th May 2025,
Accepted 8th August 2025

DOI: 10.1039/d5cc03028e

rsc.li/chemcomm

Introduction

Carbon quantum dots (CQDs), a recent and significant addition to the nanomaterial family, have emerged as a highly promising class of fluorescent nanomaterials due to their unique advantages, including excellent photoluminescence, superior photostability, minimal toxicity, outstanding biocompatibility, and relatively simple synthesis methods.¹ These advantageous

^a College of Biological and Chemical Engineering, Qilu Institute of Technology, Jinan, Shandong, 250200, China. E-mail: w.h1127@163.com, hymou@alu.ruc.edu.cn

^b State Key Laboratory of Chemical Resource Engineering, College of Chemistry, Beijing University of Chemical Technology, Beijing, 100029, China. E-mail: jibin.song@buct.edu.cn

^c Handan Kaipu Xin Technology Co., Ltd, Handan, Hebei, 075570, China



Wen He

Wen He obtained her PhD degree in Chemical Engineering at Universiti Malaysia Sarawak, Malaysia, in 2025. She is currently working at Qilu Institute of Technology. Her primary research focuses on the design and synthesis of biomass-derived carbon quantum dots.



Jibin Song

Jibin Song obtained his PhD degree in Chemical and Biomedical Engineering at Nanyang Technological University, Singapore, in 2014. He then worked as a postdoctoral fellow at the National Institutes of Health (NIH). He joined Fuzhou University as a "Min Jiang Scholar" professor of analytical chemistry in 2018. In 2022, he joined the State Key Laboratory of Chemical Resource Engineering of Beijing University of Chemical Technology as a professor and group leader of the Laboratory of Living Imaging and Analysis. His research focuses on developing molecular imaging nanoprobes for bioimaging and drug/gene delivery.

properties distinguish CQDs from conventional organic fluorescent dyes and semiconductor quantum dots, positioning them as a major research hotspot in nanotechnology. Consequently, CQDs are now widely explored and applied in diverse fields such as analysis and detection, biological imaging, optical devices, drug delivery, and photocatalysis.

The carbon sources used for synthesizing CQDs primarily fall into two categories: chemical precursors (*e.g.*, citric acid, urea, ethylenediamine, and *p*-phenylenediamine) and biomass (*e.g.*, milk, apple, aloe, and grass).² In line with the growing global emphasis on sustainability and environmental consciousness, “green” and “environmentally friendly” synthesis routes have become a preferred direction. Biomass, as a carbon source, offers significant advantages: it is green, natural, inexpensive, readily available, sustainable, and often possesses high carbon content suitable for CQD synthesis.³ Biomass-derived CQDs (BCQDs) have thus become one of the most competitive fluorescent nanomaterials, leveraging their cost-effectiveness and wide raw material base for extensive application in biosensing and biomedicine.⁴ For fluorescence detection using BCQDs, their inherent fluorescent properties enable specific interactions with target analytes to induce quantifiable changes in fluorescence signals (intensity/wavelength), and such changes exhibit a definite quantitative relationship with analyte concentrations, thereby realizing fluorescent sensing detection of targets.⁵ However, challenges remain in scaling up their commercial production, driving considerable research interest in the large-scale synthesis of BCQDs using biomass precursors.

The development of highly effective BCQD-based biosensors is particularly crucial for addressing significant public health challenges. Fluorescence analysis constitutes a robust and extensively employed technique for quantitative assessment in the fields of environmental monitoring and medical diagnostics due to its high selectivity, sensitivity, and cost-effectiveness.⁶ However, a major limitation is that most target ions (*e.g.*, heavy metal ions) and small biologically active molecules are inherently non-fluorescent. Their detection typically requires indirect measurement using external fluorescent probes. This creates a critical need for specific, targeted fluorescent probes like BCQDs.

This need is underscored by the severe health impacts of imbalances in these analytes. For instance, mercury ions have the potential to inflict substantial harm on the pulmonary, renal, nervous, digestive, and immune systems, with excessive exposure posing a risk of fatality.⁷ While copper is a crucial trace element necessary for the proper functioning of enzymes, the coagulation of blood, the maturation of hormones, and the metabolism of cellular energy (with adults typically containing 100–200 mg),⁸ excessive levels can be cytotoxic. Similarly, enzymes such as the ubiquitous hydrolase pyrophosphatase play a critical role in processes including bone formation, glucose metabolism, and DNA synthesis⁹ and molecules like reduced glutathione (critical for antioxidation and toxin clearance) or elevated levels of biomarkers like neutrophil gelatinase-associated lipocalin (NGAL, indicating conditions such as

Table 1 Limit values for metal ions in daily drinking water

Metal ion	China (mg L ⁻¹)	United States of America (mg L ⁻¹)	European Union (mg L ⁻¹)
Arsenic	0.01	0.01	0.01
Cadmium	0.005	0.005	0.01
Chromium	0.05	0.1	0.05
Lead	0.01	0.015	0.01
Mercury	0.001	0.002	0.001
Selenium	0.01	0.05	0.01
Aluminum	0.2	0.05–0.2	0.2
Iron	0.3	0.3	0.3
Manganese	0.1	0.05	0.05
Copper	1.0	1.3	2.0
Zinc	1.0	5	—

hepatitis, pneumonia, AIDS, or cancer),¹⁰ require precise monitoring. Consequently, accurately identifying the concentrations of heavy metal ions and biologically active compounds is vital for diagnosing and treating associated diseases. National standards further mandate strict limits on metal ion concentrations in essentials like drinking water (Table 1), highlighting the practical necessity for reliable detection methods.¹¹

Therefore, there is a compelling demand to develop rapid, effective, sensitive, and specific biosensors based on BCQDs for the detection of these critical analytes. This review comprehensively summarizes the carbon sources, fundamental properties, synthesis methods, luminescence mechanisms, sensing mechanisms, elemental doping strategies, and the latest progress in the biosensing applications of BCQDs. Furthermore, it identifies current research gaps and proposes future development directions for this promising field.

Carbon sources of BCQDs

In a circular economy, it is important to transform significant amounts of biomass waste into materials and energy sources that add value, in order to decrease pollution, lower atmospheric CO₂ levels, and reduce waste disposal expenses. However, a lot of individuals focus solely on the characteristics and uses of CQDs, overlooking the significance of carbon sources. Nature provides almost all of these natural resources, and biomass is safer, less expensive, and more readily available than toxic organic molecules such as aromatic hydrocarbon compounds. Therefore, biomass is a good carbon source for the preparation of CQDs.

Biomass is any material of plant or animal origin that can be used as a carbon source for BCQDs.¹² Biomass has a variety of sources, from both waste and nonwaste renewable products. As shown in Table 2, various types of biomass have been used as initial carbon sources to prepare BCQDs. However, the carbon source precursors used in the preparation process, such as banana juice,¹³ marine polysaccharides,¹⁴ and chicken egg white (Fig. 1a),¹⁵ are expensive and cannot fully utilize the advantages of low cost and being a wide source of raw materials for BCQDs. Thus, the selection of an appropriate initial biomass carbon source is the key problem to be solved in the development of BCQDs.

Table 2 Preparation of BCQDs utilizing both waste and non-waste renewable materials as carbon sources

Biomass type	Carbon Source	Methods	Size (nm)	QY (%)	Applications	Detection range (μM)	Detection time (min)	Detection limit (μM)	Ref.
Non-waste renewable products	Banana juice	Hydrothermal	1.27	32	Cu(II)	16–12 588	—	4.72	13
	Chicken egg white	Base catalysis	8.4	25.6	Fluorescent ink	—	—	—	15
	Banana stem	Hydrothermal	9	15.1	Cr(VI)	10–30	0.33	2.4	16
	Eggshell membrane	Hydrothermal	8	9.6	Detecting Hg(II)	10–100	—	2.6	21
	Marine polysaccharide	Hydrothermal	<10	20.46	Bioimaging	—	—	—	22
	Fish scale collagen peptides	Hydrothermal	2.27	9.29	Biosensing	—	—	—	23
Waste renewable products	<i>Aegle marmelos</i> leaves	Microwave	6.64	14.21	Fe ³⁺	0–20	10	0.184	17
	Aloe leaves	Hydrothermal	5.64	21.4	Nitenpyram	0.5–200	10	0.15	18
	Apricot leaves	Hydrothermal	2.39	27.6	Cu(II)	0–120	5	0.65	20
	Purslane leaves	Hydrothermal	5	—	Formaldehyde (HCHO)	97–773	30	—	24
	Maple tree leaves	Hydrothermal	7.59	—	Cesium ions	0.1–100	10	0.024	25
	Peach leaves	Hydrothermal	1.9	7.71	Bioimaging	—	—	—	26
	Waste tea residue	Chemical oxidation (HNO ₃)	3.2	5.67	TC and bioimaging	0.0–7.2	15	0.09	27
	Sweet potato peels	Hydrothermal	2.0	8.9	OTC	1.1×10^{-4} – 2.0×10^{-3}	5	3.3×10^{-5}	28
	<i>Ginkgo biloba</i> L. leaves	Hydrothermal	3.5	—	Butocarboxim	0.003–0.2	10	9.7×10^{-4}	29
	Sugarcane waste	Hydrothermal	2–8	14.12	Hg(II) ion sensing and bioimaging	0–300	1	0.1	30

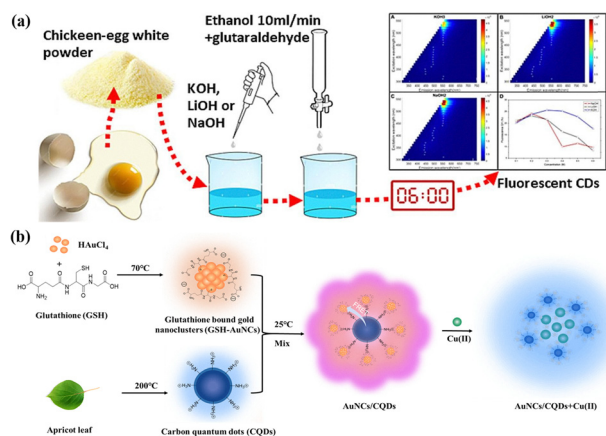


Fig. 1 BCQDs prepared from (a) chicken egg white. Reproduced with permission from ref. 15. Copyright Elsevier, 2024. (b) Apricot leaves. Reproduced with permission from ref. 20. Copyright Taylor & Francis, 2025.

Waste biomass, defined as discarded organic materials originating from agriculture, forestry, or daily life (such as food scraps, leaves, and residual agricultural materials), is seen as the most eco-friendly option and not only contributes to waste management but is also usually less costly. In recent years, an increasing number of people have used leaves as a biomass carbon source to prepare BCQDs. BCQDs with an intense bright blue emission band near 447 nm were prepared from banana stems. Their quantum yield (QY) reached 15.1%. Cr(VI) can be detected in the linear detection range (10–30 μM) with a detection limit (LOD) of 2.4 μM .¹⁶ Rani *et al.*¹⁷ prepared BCQDs from *Aegle marmelos* leaves for detecting Fe³⁺ with high selectivity. The linear range of Fe³⁺ was 0–20 μM , with a LOD of 0.18 μM . However, in China, compared with *Aegle marmelos* leaves, aloe vera leaves have the advantage of being suitable for all seasons. Wang *et al.*¹⁸ prepared BCQDs based on Aloe vera leaves and combined them with glutathione-encapsulated

copper nanoclusters to construct ratiometric fluorescent probes for detecting allylcarbamate. The linear range of allylcarbamate was 0.5–200 μM , with a LOD of 0.15 mM.

As shown in Table 2, various types of leaves have been used as carbon sources to prepare BCQDs. However, no one has prepared BCQDs using apricot leaves as carbon sources. However, apricot trees are planted in more than 60 countries around the world.¹⁹ Therefore, using apricot leaves as carbon sources to prepare biomass CQDs can effectively lower the cost and realize the high-quality recycling of biomass resources. For the first time, our team prepared BCQDs from apricot leaves and synthesized AuNC/CQD ratio fluorescent probes (Fig. 1b). The specificity and stability of the AuNC/CQD ratiometric fluorescent probe and its application in real water samples were investigated. The linear range of the AuNC/CQD ratiometric fluorescent probe for Cu(II) was 0–120 $\mu\text{mol L}^{-1}$, the R^2 value reached 0.9982, and the LOD was 0.65 $\mu\text{mol L}^{-1}$. Compared with those of other Cu fluorescent sensors, the linear range of this probe was wide, and the LOD was low.²⁰

Properties of BCQDs

Typically, BCQDs consist of a sp^2 or sp^3 hybrid carbon core,³¹ and their surface functional groups commonly include hydroxyl, carboxyl, and epoxy groups, which make them highly water soluble.³² However, the varying crystallinity and intricate microstructure of BCQDs result in diverse properties. The basic characteristics of BCQDs include the following three areas.

UV-visible absorption properties

BCQDs created using various techniques have distinct chemical compositions, typically exhibiting significant absorption capabilities in the ultraviolet spectrum, generally between 230 and 330 nm,³⁰ and extend to the wavelength range of visible light. The UV-visible absorption characteristic peaks of the BCQDs are mainly influenced by the species of surface groups, the size

Highlight

of the π - π -conjugate structure, and the O/N content ratio in the carbon core.³³ For instance, the UV spectrum of BCQDs prepared by the hydrothermal method revealed two distinct peaks at 242 nm and 310 nm, which are caused by the π - π^* transition of the C=C bond and the n - π^* transition of the C=O bonds, respectively. The absorption peak of the BCQDs prepared by pyrolysis redshifted to 335 nm,³⁴ and the width of the half-peak decreased. The surface functionalization also affects the UV-vis absorption. For instance, the absorption spectra of the amine-functionalized CQDs are significantly redshifted and appear in the 300–600 nm region.

Fluorescence properties

The fluorescence properties are among the most remarkable properties of BCQDs. By utilizing different fluorescent substances, such as cadmium or lead, in traditional quantum dots, rare earth nanomaterials, and organic small molecule dyes, BCQDs exhibit superior light stability and quality, increased fluorescence QY, reduced toxicity, improved biocompatibility, abundant low-cost resources, and extensive applications. The luminescence of BCQDs consists of both downconversion photoluminescence and upconversion photoluminescence.³⁵ The first type of luminescence is referred to as Stokes luminescence, while the second type is known as anti-Stokes luminescence. The former occurs when the emitted wavelength is longer than the excitation wavelength, whereas the opposite is true for the anti-Stokes luminescence. The mechanism of upconversion luminescence usually occurs when the electrons of CQDs absorb multiple photons simultaneously, leading to their excitation to higher vibrational levels. However, the opposite trend was observed for the downconversion photoluminescence.

Typically, BCQDs emit blue or green fluorescence, which restricts their biomedical applications. Recently, numerous research studies have created BCQDs that produce red or near-infrared fluorescence. Red BCQDs were prepared by an ultrasound-assisted method at room temperature using perilla as a precursor.³⁶ Its emission peak was concentrated at 670 nm with a QY of 28%. Qin's team firstly reported that the red fluorescence of leaf-derived carbon dots originates from chlorophyll and that new luminescent centers of BCQDs can be tuned by controlling the temperature of the solvothermal reaction. This work provides unprecedented insights into the luminescence mechanism of BCQDs.

On the other hand, because high-color-purity carbon quantum dots have relatively large advantages in bioimaging and photoelectric devices, scientists have been researching CQDs that have limited emission ranges.³⁷ Previous studies have reported that the full width at half-maximum (FWHM) of some CQDs ranges from 20–40 nm.³⁸ Yuan *et al.*³⁸ synthesized a series of multicolor luminous CQDs with a FWHM of 30 nm, which did not depend on the excitation wavelength. The synthesized CQDs have high crystallinity and a unique rigid triangular structure, and a large number of hydroxyl groups on their surface can cause weak electron-photon interactions, which results in high color purity. Liu *et al.*³⁹ prepared BCQDs using the leaves of *Picea abies* as precursors with a FWHM of

20 nm and an emission wavelength of 673 nm. The QY of these deep red light BCQDs reaches 59%. The results show that the QY is increased and the FWHM is decreased by the N-doped heterocycle and the extensive conjugate system.

Moreover, most BCQDs have an excitation wavelength dependence, which is the phenomenon in which the fluorescence emission wavelength redshifts as the excitation wavelength increases. This is possibly because of the multiple fluorescence emission centers of BCQDs and the wide distribution of different energy levels. Therefore, BCQDs have the ability to alter the wavelength of their fluorescence emission by adjusting the excitation wavelength, without any modifications to their chemical composition or dimensions, which greatly facilitates their applications in multicolor fluorescence biological imaging.

Phosphorous light properties

Room-temperature phosphorescence (RTP) is a unique property of CQDs. RTP is generated by two main mechanisms: (i) the shift from the excited singlet state (S_1) to the triplet state and (ii) the emission from the lowest excited triplet state (T_1) to the ground state. Additionally, heightened spin-orbit coupling can aid in exciton transitions from singlet to triplet states to increase RTP generation. Moreover, inhibiting the nonradiative transition of the triplet exciton also plays a crucial role in RTP production.⁴⁰ RTP materials have been widely used in bioimaging, biosensing, and optical devices. Conventional RTP materials typically consist of inorganic or metal complexes, but their drawbacks, such as high toxicity and cost, significantly restrict their potential uses. Biomass, as a natural, abundant and renewable carbon resource, has been used to prepare RTP BCQDs.⁴¹

RTP BCQDs were prepared using *Schisandra chinensis* polysaccharides as the only carbon source.⁴² The RTP BCQDs exhibited lifetimes as high as 271.2 ms at $\lambda_{\text{ex}} = 350$ nm and a small energy gap (0.32 eV). Additionally, they show sufficient quenching with Fe^{3+} . The observable RTP intensity decreased as the concentration of Fe^{3+} increased within the range of 0.1–2 mM, with a LOD of 0.57 μM . Zhang's team⁴³ prepared NL-CDs based on carboxymethylated lignin, the NL-CDs were confined in SiO_2 , and the generated NL-CDs@ SiO_2 showed excellent phosphorescence behavior in both solid-state and aqueous solutions. The obtained afterglow material achieved a phosphorescence QY of 5.97% and a lifetime of 834 ms. This scheme provides guidance for the high-value utilization of lignin. BCQDs were prepared from wheat straw, and boron-doped carbon dots (CDs@IPA) with IPA shells were obtained by doping with an elemental boron and isophthalic acid (IPA) coating.⁴⁴ CD@IPA irradiated with UV lamps of different wavelengths showed different solid fluorescence, whereas turning off the UV lamps produced green visible RTP, which lasted for 5 s and was visible to the naked eye (Fig. 2). The bifunctional luminescent properties of these straw-based carbon dots can be used to detect Cu^{2+} and as RTP anticounterfeiting markers to ensure information security. For the first time, the RTP emission of coal-based humic acid-derived carbon dots (HACDs) in

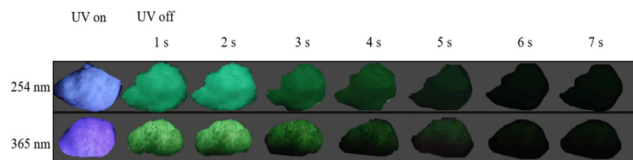


Fig. 2 Fluorescence images of CDs@IPA under the excitation of 254 and 365 nm UV light, and phosphorescence image after ceasing the excitation of 254 and 365 nm UV light for 1–7 s. Reproduced with permission from ref. 44. Copyright Elsevier, 2022.

boric acid has been realized.⁴⁵ The results showed that boron-carbon bonds were easily generated between the HACDs and boric acid under heating conditions. In addition, the prepared HACDs contained a large number of phenolic hydroxyl groups on the surface, which were easily oxidized to carbonyl groups by hydrogen peroxide, thus improving the phosphorescence lifetime. The resulting RTP material exhibited an ultralong phosphorescence lifetime of 632.20 ms and an excellent afterglow of up to 9.0 s with a phosphorescence QY of 7.6%. This work provides guidance for identifying abundant and cost-effective carbon sources on Earth and a new method for regulating the emission mechanism of coal-sourced carbon dots.

Currently, the preparation and application of BCQDs with RTP are still in the early stages of research. In the future, the fluorescence QY, phosphor afterglow lifetime, and stability of BCQDs should be improved by studying the reaction raw materials, pretreatment methods, and reaction conditions.

Preparation of BCQDs

Various BCQDs have been synthesized from natural products (*i.e.*, orange juice, coffee grounds, silk, green tea, eggs, eggshell film, soybean milk, flour, bananas, sweet peppers, honey, coriander leaves, garlic, bergamot, aloe, lemon juice, pear juice, hair, *etc.*) or waste materials (*i.e.*, waste paper, paper ash, petroleum coke, *etc.*) as precursors.⁴⁶ Two primary synthesis techniques commonly employed are known as the “top-down” and “bottom-up” methods.⁴⁷ The “top-down” approach involves utilizing physical or chemical techniques such as chemical oxidation and electrochemical synthesis to transform large sp^2 carbon structures into smaller CQDs. While these techniques are straightforward, user friendly, and efficient in terms of time, they are only applicable to materials containing extensive sp^2 carbon structures, such as graphene, carbon fiber, and carbon black. Although this method cannot accurately control the size and shape distribution of the product, it is precise because of the diversity of sizes and shapes, and it also provides an opportunity for the development of CQDs with adjustable emission wavelengths. The “bottom-up” approach involves utilizing small molecules as precursors for carbon sources to prepare CQDs by hydrothermal methods and microwave-assisted methods. This method enables organic molecules to form sp^2 carbon domains through intermolecular coupling during carbonization to form CQDs whose size and morphology can be controlled. Although this method has the

disadvantage of being time-consuming and complex, the synthesized CQDs are relatively uniform in size and controllable in morphology, and the requirement for carbon sources is relatively low. This paper will introduce the following two main types of methods.

Hydrothermal method

The hydrothermal method refers to the preparation of products by high-temperature polymerization and carbonization of precursor molecules. The reaction is easy to control and causes little environmental pollution. It is considered to be a direct and effective method for material preparation.³⁷ The properties of the BCQDs derived from various carbon sources and prepared using hydrothermal methods are presented in Table 2. The QYs of most biomass CQDs without functionalization are generally low (less than 10%), which seriously limits their applications in biosensing and bioimaging.

Zhang *et al.*⁴⁸ produced fluorescent CQDs for the first time using a hydrothermal technique. Zhao *et al.*⁴⁹ synthesized blue fluorescent nitrogen-sulfur codoped BCQDs by a hydrothermal reaction using garlic as a carbon source precursor. In contrast to certain conventional fluorescent dyes, BCQDs demonstrate outstanding optical characteristics, good chemical and photochemical stability, and excellent biocompatibility, so they are ideal visual probes for imaging both *in vivo* and *in vitro*. Furthermore, the CQDs also exhibit effective scavenging of free radicals, demonstrating their multifunctional applications in biological imaging and antioxidation. Ding *et al.*⁵⁰ synthesized red fluorescent BCQDs in high yield (28%) by a hydrothermal method using lemon juice and ethanol as the raw materials. The typical size of the red fluorescent BCQDs was measured to be 4.6 nm, and the emission wavelength at 631 nm was independent of the excitation wavelength. At the same time, the BCQDs have low cytotoxicity and good photostability. Given their environmentally friendly synthesis methods and good optical properties, BCQDs show great potential for use in bioimaging and light-emitting diodes. Wei *et al.*⁵¹ used natural *Gynostemma pentaphyllum* as a carbon source precursor, synthesized blue fluorescent CQDs with an average particle size of approximately 2.5 nm and good dispersion using a high-temperature hydrothermal method, and evaluated the biotoxicity of the CQDs using zebrafish embryos. The findings indicated that 90% of zebrafish embryos successfully hatched and survived when exposed to CQDs, with less than 10% showing deformities. This suggests that the BCQDs demonstrated favorable biocompatibility. In addition, the BCQDs promoted the mRNA expression of related genes in zebrafish, encoded more antioxidant proteins, and had both imaging and therapeutic effects. Studies have shown that fluorescent BCQDs are potential candidates for the biological imaging and treatment of diseases caused by excessive oxidative damage, such as cancer, aging, and other aging-related diseases.

A biomass nitrogen-doped blue fluorescent CQD fluorescence sensor for Cr(VI) detection was synthesized using longan fruit peel.⁵² There was a good linear relationship between the photoburst rate of the sensor and the concentration

Highlight

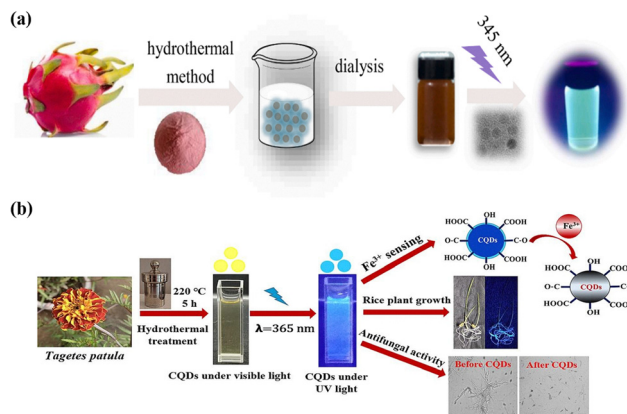


Fig. 3 Preparation of BCQDs from (a) papaya peels. Reproduced with permission from ref. 53. Copyright Elsevier, 2024. (b) *Tagetes patula*. Reproduced with permission from ref. 55. Copyright Elsevier, 2023.

(20–200 μM) of the detected samples. The detection limit was 1.4 μM . Effective and environmentally friendly BCQDs were prepared from papaya peels using a hydrothermal method.⁵³ Physicochemical characterization revealed that the particle size and carbon content of the BCQDs varied with the preparation time (Fig. 3a). BCQDs (FS-CDs) with an average diameter of 2.52 nm were prepared using fish scales as a carbon source.⁵⁴ They not only exhibited excitation-dependent emission but also quantum efficiencies of up to 31.71%. The high photoluminescence QY of FS-CDs is associated with (N, O) codoping and a high doped nitrogen content. In addition, the FS-CDs exhibited significant fluorescence imaging capabilities in zebrafish. BCQDs with an average particle size of approximately 5.15 nm were synthesized based on *Tagetes patula* with a QY of 29.88%.⁵⁵ The synthesized BCQDs were used as sensing probes for the detection of Fe³⁺ with a linear range of 0–4 μM and LOD of 0.32 μM (Fig. 3b). BCQDs based on *Acorus calamus* with an average particle size of 6 nm, blue fluorescence under UV irradiation up to 360 nm, and a QY of 15% were prepared from rhizomes.⁵⁶ Based on the static and internal filtration effect, the developed radio-sensors exhibited high selectivity for mulberry pigments, with a linear range of 0–2 μM and LOD of 96 nM. The catalytic reduction of the ionic dyes Rh B and SY was achieved in a few seconds using NaBH₄-CQD mixtures. The reaction followed quasi-primary kinetics with a rate constant of 0.0116 min. Cytotoxicity studies revealed the anticancer ability of CQDs against the SKMEL 28 cell line with a LOD as low as 102 $\mu\text{g mL}^{-1}$.

Overall, the hydrothermal method refers to the preparation of products by high-temperature polymerization and carbonization of precursor molecules. The advantage of this method is good control of the particle size and morphology, but it involves complex procedures.

Microwave method

Microwave-assisted synthesis is an efficient and time-saving method. Ichthyotic collagen peptides were utilized as precursors to synthesize CQDs via hydrothermal (CQDs-HT) and microwave (CQDs-MW) techniques.²³ Researchers have compared the optical

characteristics of CQDs produced using two different methods and analyzed how the heating process affects the structure of the CQDs. Both types of CQDs emit blue light and exhibit emission properties that depend on the excitation. Moreover, microwave heating is rapid and uniform, which is more favorable for N self-doping. While the N doping in CQDs-HT is minimal, there is a high proportion of pyrrole N present. In contrast to the limited sealing ability of microwave reaction vessels, the traditional hydrothermal method provides a controlled high-temperature sealing environment that facilitates thorough dehydration and condensation of the precursors, resulting in the formation of smaller CQDs. Thus, compared with CQDs-MW, CQDs-HT exhibited a greater QY (9.29% vs. 4.86%) (Fig. 4a).

Rodriguez-Padron *et al.*⁵⁷ synthesized blue fluorescent BCQDs with a particle size of 17.5 nm by a microwave-assisted method using lignocellulose residue in wood pulp as the raw material. This study shows the application prospects of these materials for the conversion of waste materials into useful fluorescent nano-materials. BCQDs doped with multiple elements from eggshell biomass waste were prepared for fluorescence determination of molnupiravir,⁵⁸ a COVID-19 antiviral drug, using a microwave method for only 90 seconds (Fig. 4b). The resulting BCQDs exhibited maximum blue fluorescence emission at λ_{em} 408 nm upon excitation at λ_{ex} 340 nm. The probe showed good linearity for the detection of molnupiravir in the range of 2.5–70 $\mu\text{g mL}^{-1}$. BCQDs with an average size of 10.12 nm and a QY of 6.01% have been synthesized from Arabica coffee powder activated carbon and were successfully used as fluorescent sensors for detecting Fe³⁺, Pb²⁺ and Cr³⁺. The CQDs were fabricated using microwave heating for 5–10 minutes, and when exposed to 365 nm excitation, the CQDs emitted bright blue light at 455 nm.⁵⁹ P-BCQDs with a size of approximately 5 nm and a QY of 33% were prepared via a microwave method with sweet lime. By employing a fluorescence burst mechanism, this was facilitated by interactions involving functional groups and surface traps through energy transfer

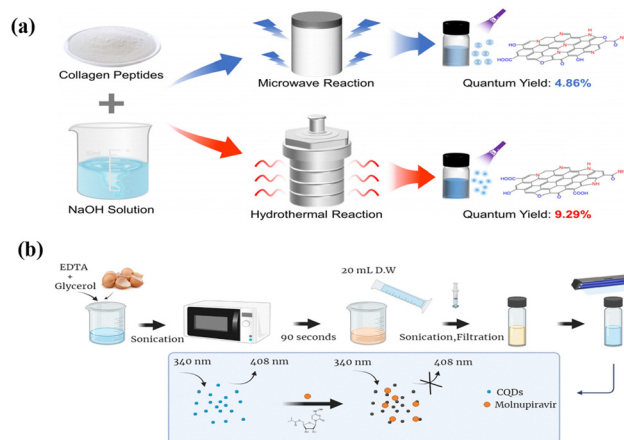


Fig. 4 (a) Variances in the production of CQDs through traditional hydrothermal and microwave techniques. Reproduced with permission from ref. 23. Copyright Royal Society of Chemistry, 2023. (b) CQDs with multidoped elements from eggshell biomass waste for the fluorometric determination of molnupiravir. Reproduced with permission from ref. 58. Copyright Elsevier, 2024.

interactions between the carbon dots and metal ions. Impressively, P-BCQDs exhibit a low detection limit of 51 nM for Fe^{3+} and 81 nM for Hg^{2+} . In addition, it demonstrated the ability to degrade methyl orange dye, achieving 70% degradation efficiency in only 240 min under normal visible light without further fusion with other materials. Thus, the study of P-BCQDs demonstrates great dual potential and efficiency for environmental applications.⁶⁰ The blue-emitting carbon quantum dots of biomass, S,N-CQDs ($\lambda_{\text{ex}}/\lambda_{\text{em}}$ 340/418 nm), which are renewable, inexpensive, and green carbon sources and self-passivators, were synthesized with a QY of 15.2% via a 4-minute microwave treatment of onion and cabbage juices.⁶¹ A thorough analysis of naturally sourced quantum dots made from biomass revealed the presence of self-doping with nitrogen and sulfur. These S,N-CQDs can serve as fluorescent markers for accurately and sensitively detecting nitazoxanide within the concentration range of 0.25–50.0 μM , with a LOD of 0.07 μM . The recoveries were as high as $98.14 \pm 0.42\%$. In addition, the Hb concentration ranged from 36.3 to 907.5 nM, with a minimum detection rate of 10.30 nM.

Compared to hydrothermal reaction times of a few hours or a dozen hours, microwave-assisted synthesis enables the rapid preparation of BCQDs; however, this approach typically results in BCQDs exhibiting heterogeneous particle size distributions.⁶² Moreover, the production yields (mass ratio of obtained CQDs to raw materials) of different raw materials vary under these two methods. Benefiting from controllable carbonization in a closed environment with moderate temperature, the hydrothermal method shows relatively low yields for complex or hardly hydrolysable biomass. For instance, the production yield is only 6.8% when durian pulp is used as the raw material.⁶³ It is more suitable for biomass rich in easily hydrolysable components. For example, the yield of the hydrothermal method can reach 55% with corncob as the raw material,⁶⁴ making it the preferred method for high-yield preparation. The microwave method, featuring rapidity and energy efficiency, is suitable for small-molecule raw materials or pre-treated biomass (such as carbohydrate⁶⁵ and organic acids⁶⁶), with a moderate production yield (10%–30%).⁶⁷ However, limited by the complexity of raw materials and heating uniformity, it is difficult to achieve ultra-high yields, and thus is more suitable for scenarios requiring rapid synthesis. The essential reason for the yield difference between the two methods lies in their reaction mechanisms. The hydrothermal method retains the carbon skeleton through a balance of slow hydrolysis and carbonization, while the microwave method relies on polymerization reactions initiated by rapid molecular vibration. The accessibility of raw materials (the ease with which carbon sources in raw materials are contacted, activated and converted into CQDs precursors by the reaction system) and the matching of reaction parameters are the core factors determining the production yield.

Luminescence mechanism of BCQDs

The luminescence mechanism of BCQDs is closely related to their preparation process. BQDs prepared from different raw

materials, different preparation methods, and different pre-treatment methods usually have different components and structures, which can lead to different optical properties. Currently, the most recognized BCQD fluorescence mechanism involves a quantum domain effect, surface-state luminescence, and molecular-state luminescence.

Quantum-restricted domain effect

BCQDs typically have a size smaller than 10 nm, so some researchers speculate that, similar to the luminescence mechanism of quantum dots, the luminescence performance of BCQDs is also related to the quantum confinement effect.⁶⁸ When semiconductor crystals are nanoleveled, the grain boundaries have a significant effect on the electron distribution within the crystal, which leads to the occurrence of energy relaxation dynamics related to the band gap and size,⁶⁹ which is the quantum limit effect.

Yuan *et al.*⁷⁰ synthesized a series of CQDs emitting different wavelengths of fluorescence (blue, green, yellow, orange, and red light, using citrate and diaminobanaphthalene) by changing the reaction conditions. Unlike most previously reported CQDs, these CQDs have no excitation wavelength dependence, high surface passivation, high crystallinity, and high fluorescence QY (75%). By analyzing their spectra, their UV-visible absorption wavelengths were 350 nm, 390 nm, 415 nm, 480 nm, and 500 nm (Fig. 5a), which coincide with the corresponding maximum fluorescence excitation wavelengths, indicating that their fluorescence emission comes from the bandgap transition. Moreover, TEM revealed that these CQDs have different particle sizes (1.95–6.68 nm). With increasing particle size, the fluorescence emission redshifted (430–604 nm), which revealed that the fluorescence of the CQDs came from the quantum domain effect. Jiang *et al.*⁷¹ prepared three CQDs with particle sizes of 6 nm, 8 nm, and 10 nm, emitting blue, green, and red fluorescence, respectively, which is consistent with the characteristics of the quantum domain effect. Li *et al.*⁷² and Peng *et al.*⁷³ synthesized CQDs with size dependence and quantum domain effects by electrochemical oxidation and chemical oxidation, respectively.

Surface-state luminescence

The surface state (surface oxidation degree and surface functional groups) is closely related to the optical properties of a material. The process of chemical decomposition of carbon-based materials or the polymerization/carbonization of small molecule precursors is usually an essential step for the preparation of CQDs. This highly activated process (surface oxidation and local carbonization) makes the chemical structure of the CQD surface very diverse and complex, including sp^2 hybridized carbon, sp^3 hybridized carbon, surface traps, and various functional groups.⁷⁴ Many studies have shown that the fluorescence intensity of CQDs is related to the degree of oxidation on the surface and that the intensity of the fluorescence emitted during surface oxidation increases. This is because the greater the degree of oxidation of the CQD surface, the more traps there are on the surface, and the more excitons

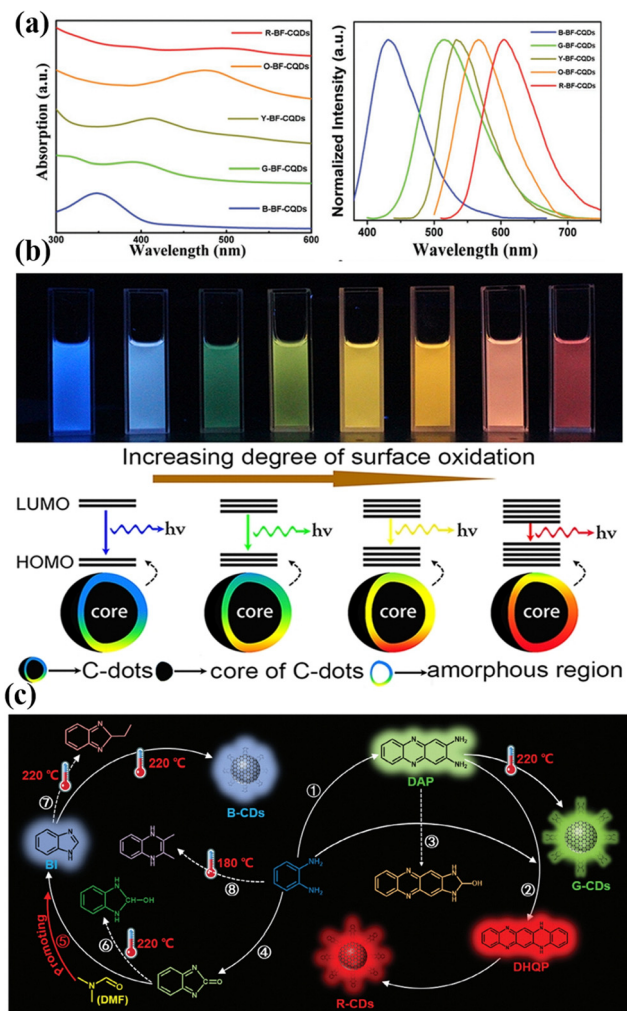


Fig. 5 (a) UV-vis absorption and normalized PL spectra of CQDs. Reproduced with permission from ref. 70. Copyright Wiley-VCH, 2017. (b) Photoluminescence phenomena of CQDs with different oxidation degrees. Reproduced with permission from ref. 76. Copyright American Chemical Society, 2016. (c) Preparation of three-color CQDs via a solvent regulation method. Reproduced with permission from ref. 80. Wiley-VCH, 2024.

will promote exciton recombination to produce radiation.⁷⁵ Ding *et al.*⁷⁶ prepared CQDs *via* a one-pot water heat method using urea and *p*-phenylenediamine and subsequently purified a series of CQDs emitting blue, green, yellow, and red fluorescence. TEM images show that the average particle size of the CQDs that emit different colors of fluorescence is 2.6 nm, which indicates that the fluorescence of the prepared CQDs does not come from the quantum domain effect. In addition, by analyzing the FT-IR and XPS spectra of the CQDs, it was found that the wavelength at which fluorescence is emitted will red-shift as the number of hydroxyl groups and the oxygen content of the carbon quantum dot surface increase. This is because when the oxygen content on the surface of the CQDs increases, the difference in the energy levels between the highest occupied molecular orbital and the lowest unoccupied molecular orbital decreases (Fig. 5b).

Zhang *et al.*⁷⁷ prepared CQDs from citrate amine and ethylenediaminetetraacetic acid *via* a solvothermal method and synthesized a series of CQDs emitting blue, green, white, yellow, orange, and red fluorescence by changing the ratio of citrate amine to ethylenediaminetetraacetic acid. By analyzing the TEM electron microscope map, the FTIR spectrogram, and XPS energy spectrum of the resulting CQDs, it was found that they had the same particle size and oxygen content. However, they differ in their amide group content, and their emission fluorescence redshifts as the concentration of the amide groups increases. The increase in the N to functional group content narrowed the energy gap and redshifted the emission fluorescence.

Molecular luminescence

Molecular luminescence originates from the electronic transitions of fluorescent molecular groups on the surface or within CQDs. These fluorophores are formed *via* precursor condensation/polymerization during synthesis. Song *et al.*⁷⁸ successfully isolated the molecular fluorophore 1,2,3,5-tetrahydro-5-oxoimidazo [1,2- α]pyridine-7-carboxylic acid (IPCA) from blue-emitting CDs, demonstrating that the primary photoluminescence centers and excitation-independent emission characteristics are attributed to IPCA. Cao *et al.*⁷⁹ first confirmed the structures of two molecular fluorophores, 2,3-diaminophenazine (DAP) and 2-amino-3-hydroxyphenazine (AHP), through purification of *o*-phenylenediamine-derived CDs. Li *et al.*⁸⁰ systematically elucidated the molecular luminescence mechanism of multicolor CDs prepared using *o*-phenylenediamine (*o*-PD) as a precursor. They found that blue, green, and red fluorescent CDs can be directionally synthesized by adjusting the ethanol/DMF solvent ratio. The luminescence arises from surface-bonded molecular fluorophores, where benzimidazole (BI), DAP, and 5,14-dihydroquinoxalinophenazine (DHQP) dominate the blue (410 nm), green (540 nm), and red (600/650 nm) emissions, respectively. Their spectral properties, fluorescence lifetimes, and pH responses closely match those of the corresponding CDs. As shown in Fig. 5c, solvent regulation revealed that pure ethanol promotes the DAP \rightarrow DHQP pathway to generate red-emitting CDs; adding DMF (>10%) inhibits DAP formation, leading to green-emitting CDs; a high DMF ratio (>50%) enriches BI to form blue-emitting CDs. This work provides direct evidence for the molecular luminescence mechanism of CDs and highlights the universal value of solvent engineering in precisely controlling the directional synthesis of fluorophores.

Finally, it should be emphasized that the luminescence of CQDs is never governed by a single effect, but rather by the synergy and competition of multiple luminescent mechanisms, which is determined by the complex structure of CQDs. Additionally, environmental effects, such as temperature,⁸¹ solvent,⁸² and pH,⁸³ can also induce variations in the luminescent performance of CQDs. Therefore, it is of great significance to dialectically understand the luminescent mechanisms of CQDs by combining their chemical composition with the influence of environmental factors.

The fluorescence sensing mechanism of BCQDs

BCQDs exhibit minimal toxicity, strong photostability, and impressive biocompatibility. In addition, their small size, large specific surface area, and abundant surface functional groups make carbon quantum dots highly reactive, making them suitable for application as fluorescent probes in fluorescent sensors. Changes in the surrounding environment, such as changes in temperature, ionic strength, and solvent conditions, may all affect the optical properties of BCQDs. The principle of a fluorescence sensor based on BCQDs is that the recognition components on the BCQDs interact with the target analyte, causing a change in its fluorescence properties, and this change has a quantitative linear relationship with the concentration of the target analyte. According to the different fluorescence signals, fluorescence sensors based on BCQDs can be divided into three types: quenching type, enhanced type, and ratio type.

Quenched type

The mechanisms of quenched fluorescent sensors can be divided into static quenching effect (SQE), dynamic quenching effect (DQE), photoinduced electron transfer (PET), fluorescence resonance energy transfer (FRET) and inner filter effect (IFE). Here, we introduce them one by one.

Static quenching effect

The SQE is the process of carbon quantum dots reacting with a quencher to generate a nonfluorescent ground state complex. When the static quenching effect occurs, (1) the fluorescence life of the BCQDs does not change significantly; (2) the UV-visible absorption spectrum of the non-CQDs is displaced during the reaction process; and (3) the temperature increase decreases the stability of the ground state complex, thus inhibiting the static quenching process and resulting in the gradual recovery and enhancement of the fluorescence intensity. The chemical interaction between the BCQDs and the quencher is one of the essential conditions for the static quenching effect, so the surface functionalization of the BCQDs favors the generation of the static quenching effect.⁸⁴

Nitrogen-doped CQDs (N-CQDs) were prepared from dried grapefruit peel for the determination of lemon yellow, which exhibited blue fluorescence with a QY of 28%.⁸⁵ The fluorescence decay curves were fitted to the aqueous N-CQDs added to lemon yellow, and the lifetimes were unchanged, indicating that the sensing principle of N-CQDs is through the SQE.

N-CQDs based on *aloe carazo* leaves emit bright blue fluorescence with a QY of 21.4%.¹⁸ In contrast, the glutathione-encapsulated copper nanoclusters (GSH-CuNCs) exhibited strong red fluorescence. A blue/red dual emission was developed using a combination of N-CQDs and CuNCs for detecting enidiamide. The spectral overlap between the UV-vis absorption of nitenpyram and the excitation of N-CQDs and the almost constant fluorescence lifetime indicated that IFE occurred in the dual-emission fluorescent probe. Furthermore, the static quenching behavior of N-CQDs/CuNCs was confirmed by the

Stern–Volmer constants ($K_{sv} = 6.92 \times 10^3 \text{ M}^{-1}$), temperature variations, and UV-vis absorptions before and after the introduction of aldicarb. Hence, the fluorescence bursting of N-CQDs caused by aldicarb is believed to result from the combined impact of the IFE and the static bursting principle.

BCQDs were synthesized *via* a simple hydrothermal process using mustard seeds as the carbon source.⁸⁶ With the formation of a nonfluorescent ground state complex between the BCQDs and Fe^{3+} , Fe^{3+} detection is achieved by an SQE. As direct evidence of the distinction between DQE and SQE, fluorescence lifetimes were also measured in the absence and presence of Fe^{3+} using time-resolved spectroscopic studies. The average fluorescence lifetime of the BCQDs was unchanged by the addition of Fe^{3+} ions, which further suggested the occurrence of the SQE mechanism. FRET and IFE can be ruled out because there is no intersection between the absorption spectrum of the quencher and the emission/excitation spectrum of the emitting BCQDs. In summary, the fluorescence quenching mechanism of BCQDs by Fe^{3+} is mainly attributed to the synergistic effect of aggregation-induced emission (AIE) and SQE (Fig. 6a).

Dynamic quenching effect

The DQE is the process of electron transfer or energy transfer between the excited CQDs and the quencher and the collision back to the ground state. Compared with the SQE, the DQE has several different characteristics: (1) the fluorescence life of the carbon quantum dot will change significantly; (2) because dynamic quenching does not generate new matter, the UV-visible absorption spectrum of the carbon quantum dot will be maintained and unchanged; (3) the quencher will not react with the carbon quantum dot; and (4) an increase in temperature will promote the dynamic quenching effect.⁸⁷

E-CQDs of *Kirinia* biomass were prepared from marine *Eucheuma denticulatum* for tetracycline (TC) detection.⁸⁸ The fluorescence intensity exhibited a strong linear correlation ($R^2 = 0.997$) within the range of TC concentrations spanning from 20 to 100 μM ; its detection and quantification limits were 0.47 μM and 1.57 μM , respectively. The mechanism of TC bursting for the fluorescence of the E-CQDs involves the IFE and DQE. The overlap between the UV-vis absorption spectra of TC and the fluorescence excitation spectra of E-CQDs leads to the absorption of the excitation light of E-CQDs by TC. This is because the fluorescence quenching mechanism of the E-CQDs is caused by the internal flocculation effect. To verify whether the fluorescence quenching of E-CQDs by TC is static or dynamic, the fluorescence lifetimes of E-CQDs before and after the addition of TC were investigated and transformed into the Stern–Volmer formula to determine the fluorescence intensity during the temperature change. K_q is the Stern–Volmer quenching constant and, according to the Stern–Volmer formula, at elevated temperatures the value of K_q is higher compared to when it is at lower temperatures. This indicates that the quenching mechanism of E-CQDs for TCs is dynamic. Furthermore, the fluorescence duration of the E-CQDs decreased from 5.74 ns to 3.57 ns following the

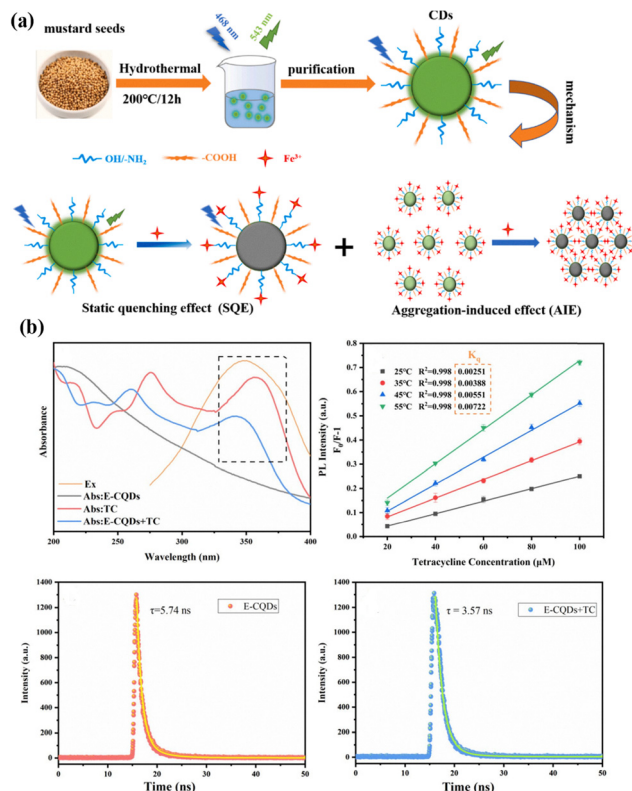


Fig. 6 (a) Preparation of CDs from mustard seeds and the mechanism of fluorescence quenching to Fe³⁺ ions. Reproduced with permission from ref. 86. Copyright Elsevier, 2022. (b) PL spectra of E-CQDs, UV-vis absorption spectra of TC, temperature correlation analysis of E-CQDs + TC, fluorescence lifetime of E-CQDs and E-CQDs + TC. Reproduced with permission from ref. 88. Copyright Springer, 2024.

introduction of TC (Fig. 6b), which further confirmed the DQE mechanism of TC on the E-CQDs.

Additionally, utilizing IFE and DQE, BCQDs with a particle size of 2.68 nm were synthesized *via* a hydrothermal method using the trunk of *Zingiber officinale* as a carbon source.⁸⁹ A correlation between the fluorescence intensity of BCQDs and the concentration of quinoline yellow ranging from 2 to 128 μmol L⁻¹ was demonstrated. A fluorescence burst clearly occurred within 1 min, with an *R*² of 0.9912 and LOD of 1.8 μmol L⁻¹.

Photoinduced electron transfer

PET is associated with the electron transfer process between excited BCQDs (electron donors/acceptors) and quenchers (electron donors/acceptors). Quenchers can form complexes with BCQDs and can excite BCQDs' doctoral state electrons back to the ground state through nonradiative emission. According to the different types of BCQDs, photoinduced electron transfer can be divided into prototype photoinduced electron transfer and oxidative photoinduced electron transfer. As the acceptor of electrons, driven by the energy gap between the lowest unoccupied molecular orbital (LUMO) and the highest occupied molecular orbital (HOMO), CQDs can accept electrons from the donor quencher by photoinduced electron

transfer. In contrast, during oxidative photoinduced electron transfer, the excited carbon quantum dots are transferred to the quencher. The oxidized photoinduced electron transfer is driven by the energy gap between the LUMO of the CQDs and the HOMO of the quencher.⁹⁰ In the photoinduced electron transfer quenching mechanism, the CQD surface is usually rich in electron-donating groups, and the quenchers are usually small organic molecules with electron-withdrawing groups.

S,N-CQDs were produced using feijoa leaves.⁹¹ When S,N-CQDs interact with dopaquinone, an electron acceptor, the fluorescence of the S,N-CQDs is suppressed. This interaction changes how electrons and holes recombine in photoexcited S,N-CQDs. S,N-CQDs contain hydroxyl and carboxyl groups that can bond with the diols, amines, and phenyl groups of L-DOPA through various mechanisms like electrostatic connections, π-π stacking, and hydrogen bonding. Functional groups like thiocyanates in S,N-CQDs are electron-rich, while dopaquinone lacks electrons. Nucleophilic functional groups can also form covalent bonds with electrophilic dopaquinone. In an alkaline solution, L-DOPA is converted to dopaquinone, which then accepts electrons from S,N-CQDs, leading to a decrease in fluorescence intensity. The difference in the average fluorescence lifetime decay of S,N-CQDs before and after adding L-DOPA suggests that the quenching process involves DQE. This mechanism induces photoinduced electron transfer between S,N-CQDs and dopaquinone, resulting in a burst of fluorescence.

Fluorescence resonance energy transfer

FRET is a process in which the excited-state energy of a carbon quantum dot used as an energy donor is directly transferred to nonradiative energy transfer with dipole-dipole coupling as a quencher of the energy receptor. This process does not produce photons, and the fluorescence emission spectrum of the CQDs overlaps with the UV-visible absorption spectrum of the quencher. Moreover, for FRET to occur, the carbon quantum dot and quencher need to be within a distance of 1–10 nm.⁹²

Murugesan *et al.*⁹³ developed novel waste-derived carbon dots using orange peel waste in combination with a FRET sensor based on a Ag nanohybrid system for the detection of melamine. CQDs and Ag nanoparticles acted as energy donors and energy acceptors, respectively. Similarly, using apricot leaves as a carbon source, our team achieved the visual detection of copper ions based on the FRET effect between BCQDs and gold nanoclusters.²⁰

Inner filter effect

Compared with other fluorescence quenching mechanisms, including FRET or PET, the IFE process has several characteristics: (1) the IFE-based sensor does not require the covalent combination of CQDs and the quencher, and the position and fluorescence lifetime of the absorption peak of the CQDs do not change; (2) there is no electron transfer or energy transfer; (3) CQDs do not require modification of surface functional groups; and (4) the distance between the carbon quantum dot and the quencher is greater than 10 nm. All of these features

make the IFE-based fluorescence sensor relatively easier to construct and more feasible. There are two modes of IFE systems. One is composed of three components: a fluorescent luminescent material, a fluorescent absorber, and an analyte. The other is made up of two components, a fluorescent luminescent material and an analyte, which is also a fluorescent absorber. The second mode greatly simplifies the operation of the experiment relative to the first mode. The eco-friendly synthesis of Fe-CQDs from waste coffee grounds was used as a peroxidase mimic for colorimetric and fluorescence detection of ascorbic acid. The absorption spectra of the Fe-CQDs + TMB + H₂O₂ system ($\lambda_{\text{ab}} = 360$ nm) overlapped considerably with the excitation spectra of the Fe-CQDs ($\lambda_{\text{ex}} = 365$ nm). Therefore, the fluorescence quenching of the Fe-CQDs may be attributed to the IFE of the TMB + H₂O₂ system.⁹⁴

Enhancement type

Enhanced fluorescent sensors are carbon quantum dots showing weak fluorescence or no emission fluorescence in the absence of an analyte. When the analyte is added, the fluorescence of the CQDs is enhanced. There are two modes of fluorescence-enhanced response: indirect and direct fluorescence-enhanced responses. In the first, the fluorescence of the CQDs is quenched by nonanalytes. When the analyte is added, the fluorescence of the CQDs is restored and indirectly enhanced. In the direct fluorescence-enhanced type, the analyte acts directly with the carbon quantum dots to enhance their fluorescence. AIE⁹⁵ and metal-induced fluorescence enhancement (MFE)⁹⁶ are the two main mechanisms of direct fluorescence enhancement in sensors. In the AIE mechanism, the groups on the surface of CQDs can coordinate with the analyte to produce aggregation, thus inhibiting the enhancement of fluorescence from the nonradiative decay process. Aggregation plays an important role in BCQD formation and fluorescence (e.g., aggregation-induced emission) but has rarely been studied in detail.

The MFE mechanism typically relies on the surface plasmon resonance (SPR) phenomenon exhibited by metal nanostructures (such as gold nanoparticles and silver nanoparticles), which increases the local electric magnetic field strength and leads to the enhancement of the surrounding CQD fluorescence. Sciortino *et al.*⁹⁷ exploited the overlap between the surface plasmon resonance of gold and the electron leaps of CQDs to achieve a fivefold increase in their fluorescence in the orange region. Ag@CQDs based on bamboo were prepared by Wang *et al.*⁹⁸ The results show that the surface plasmon resonance of Ag promotes the electron transfer properties of CQDs and thus improves the optical performance.

Ratiometric type

Most fluorescence sensors use fluorescence quenching at a single wavelength or fluorescence enhancement as the output signal for quantitative analysis, which causes the fluorescence signal to be susceptible to many analyte-independent factors, such as fluctuations in the excitation light source, probe concentration, light scattering of the sample matrix and fluctuations in the solution environment. A ratiometric-type

fluorescent sensor detects an analyte by recording changes in the ratio of fluorescence intensity at two wavelengths, which greatly reduces the impact of changes in the external factors described above.⁹⁹ Therefore, ratiometric fluorescent sensors have more reliable and accurate experimental results than those based on a single wavelength. There are two modes: the reference mode and the dynamic mode. In the reference mode, after the addition of the target analyte, a fluorescence channel without signal change can serve as the reference, while another fluorescence channel with increased, weakened, or displaced changes in the fluorescence signal can act as the output signal. In the dynamic mode, there are two dynamic fluorescence channels, and after the addition of the analyte, the fluorescence signal changes at both wavelengths, possibly through the same or opposite changes.¹⁰⁰

BL-CQDs with single-excitation and double-emission properties were prepared based on the precursor extract of fresh banyan leaves.¹⁰¹ The BL-CQDs that were created are around 1.7 nm in size, and have a structure similar to graphene, feature different hydrophilic functional groups on their surface, and exhibit strong fluorescence characteristics. The I_{677}/I_{460} were linearly correlated with ACE activity in the range of 0.02–0.8 U L⁻¹. The blue/red dual emission of N-CQDs/CuNCs mixtures based on nitrogen-doped CQDs of *Aloe carazo* leaves was established for the detection of aldicarb.¹⁸ Under 350 nm excitation, the N-CQDs/CuNCs system produced dual wavelength emission peaks at 440 and 660 nm (Fig. 7a). In addition, the fluorescence intensity of the N-CQDs significantly decreased, and that of the GSH-CuNCs slightly changed when enediamine was introduced into the system; moreover, the solution color changed from bright blue to deep red. A good linear relationship was observed between the I_{660}/I_{440} value and the concentration of aldicarb (0.5–200 μM), with a LOD of 0.15 μM . The dual-emission fluorescent probe provided satisfactory recoveries (95.0%–107.0%) for the detection of aldicarb in real water. These results were similar to those achieved using the traditional liquid chromatography-tandem mass spectrometry (LC-MS/MS) technique.

The luminescence of BCQD ratiometric fluorescent probes is mainly concentrated in the short wavelength region, and due to their weak penetration ability, most BCQD-based ratiometric fluorescent probes are currently tested for applications in aqueous solutions, while there are fewer applications for the direct determination of analytes in cells or *in vivo*.

Enhancing the quantum yield of BCQDs

Compared with traditional fluorescent dyes, the QY of CQDs from biomass is generally less than 10%, which severely limits their application prospects in bioimaging and fluorescence sensing. Heteroatom doping of CQDs not only enriches the surface fluorescence active sites of CQDs and improves their fluorescence QY but also enables the functional regulation of their fluorescence properties and effectively broadens their

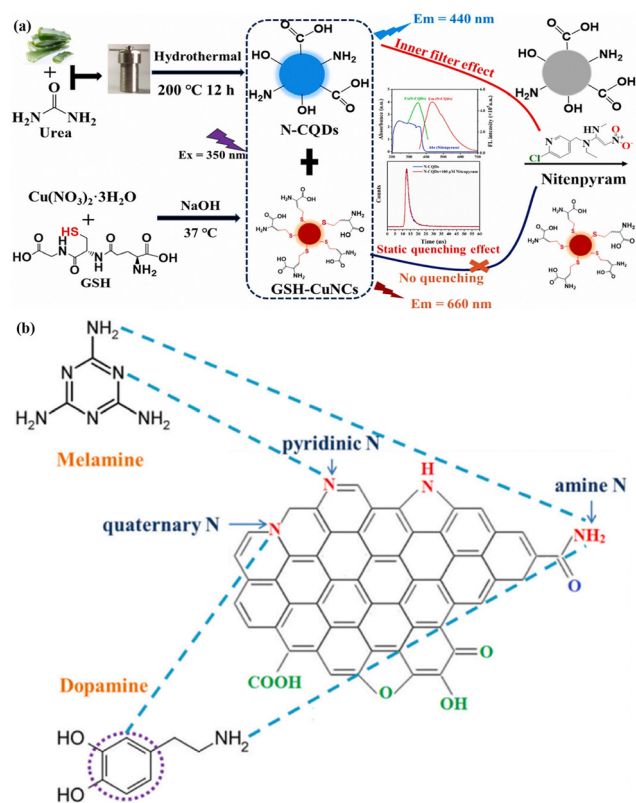


Fig. 7 (a) Synthetic route of N-CQDs/CuNCs from *Aloe carazo* leaves for detecting nitenpyram and the fluorescence spectra of the dual-emitting fluoroprobe at various nitenpyram concentrations. Reproduced with permission from ref. 18. Copyright Elsevier, 2024. (b) Schematic diagram of the chemical structure of the nitrogen sources and B-CQDs. Reproduced with permission from ref. 110. Copyright Elsevier, 2022.

application scope, which is currently the main method for the preparation of CQDs with a high fluorescence QY in biomass.

Nitrogen and sulfur are the most common doping elements in CQDs.¹⁰² Both N-doping and S-doping enhance the quantum yield by regulating the electronic structure, defect sites, and surface states of CQDs, but their underlying mechanisms are distinct.⁴³ N-doping relies more on adjusting the electron density in the skeleton and enhancing defects, while S-doping emphasizes surface chemical modification and electron conjugation effects.¹⁰³ In practical applications, high-quantum-yield doped CQDs can be achieved by selecting matched precursors, optimizing synthesis methods (such as hydrothermal method and microwave method), and tuning reaction parameters, laying a foundation for applications like fluorescent sensing.

In general, the preparation of heteroatom-doped BCQDs can be realized in the following two ways: (1) by directly selecting heteroatom-rich biomass materials as the initial carbon source and (2) by adding heteroatom-rich organic small molecules or polymers rich in heteroatoms.

Direct preparation of heteroatom-doped CQDs using biomass materials containing a large number of heteroelements reduces the number of reaction steps and is currently a popular method for enhancing the QY of biomass CQDs. As *Bauhinia* is

rich in carbon, nitrogen and oxygen, Huang *et al.*¹⁰⁴ recently prepared N-CQDs for Fe³⁺ ion detection by microwave treatment of *Bauhinia*. The QY of the prepared N-CQDs is as high as 27%, which is better than that of most biomass carbon quantum dots. In addition, nitrogen-rich Jinhua Buddha's hand,¹⁰⁵ roseheart radish¹⁰⁶ and Chinese cabbage¹⁰⁷ can also be prepared by hydrothermal reactions to obtain biomass N-CQDs with excellent fluorescence characteristics, with QYs of up to 50.78%, 13.6% and 37.5%, respectively.

Doubly doped CQDs can be prepared using biomass materials enriched with a variety of heterogeneous elements. Ye *et al.*²¹ obtained high QYs of N/S double-doped CQDs from pigeon feathers, eggshells, yolks and feces as precursors of biomass carbon sources, with QYs of 24.87% (feathers), 17.48% (eggshells), 16.34% (yolks) and 33.50% (feces), respectively. The prepared BCQDs showed high sensitivity and selective fluorescence bursts for Hg²⁺ and Fe³⁺, with LODs of 10.3 nM and 60.9 nM, respectively. In addition, Zhao *et al.*⁴⁹ reported the hydrothermal preparation of N/S double-doped CQDs using garlic, with a final fluorescence QY as high as 17.5%.

Although the direct preparation of CQDs from heterogeneous element-rich biomass materials is a relatively simple process, it can effectively improve the QY of BCQDs and broaden their application prospects. However, this method requires a high level of biomass carbon, and few biomass carbon sources are known to be available. By adding additional heteroatomic dopants, the limitations of the above method in the selection of carbon sources can be solved, and the type and content of doping elements can be adjusted according to the demand, which is the focus of this review.

Advanced NCQDs were produced through an environmentally friendly method involving hydrothermal processing, utilizing waste paper and urea as sources of carbon and nitrogen.¹⁰⁸ Compared with undoped CQDs, the single-crystalline NCQDs displayed a strong blue-green glow when exposed to UV and visible light, with a maximum increase in intensity of 6.5 times. The XPS findings showed that the increased photoluminescence was due to the existence of nitrogen from pyridine, which could be managed by changing the hydrothermal temperature, duration, and urea concentration.

Wang *et al.*¹⁰⁹ synthesized N-CQDs with a QY of up to 43.4% using the roots of *Moringa oleifera* as a carbon source and diethylenetriamine as a nitrogen source. The reason was that the nitrogen atom can regulate the charge density and spin density of the adjacent carbon atoms in the CQDs and provide new radiation pathways, which can effectively regulate the surface properties of the CQDs and thus improve the fluorescence intensity. The obtained N-CQDs were excited at 350 nm and emitted blue fluorescence at 445 nm; these N-CQDs have strong blue fluorescence, excellent anti-photo-bleaching performance and good water solubility.

Three nitrogen-doped BCQDs were prepared using cotton stalks and soybean meal as carbon sources and two reagents with different nitrogen-containing structures (dopamine and melamine) as nitrogen sources.¹¹⁰ The mechanism of the modification effect of exogenous nitrogen doping on biomass

carbon dots was discussed. Different modification effects were produced by modulating the chemical potentials of the carbon and nitrogen atoms, and these differences were reflected in the amount and state of nitrogen doping and the sp^2c structure, with dopamine playing a role in quaternary N formation (Fig. 7b). Melamine promoted the formation of pyridine N and amine N, leading to different luminescent properties (the absolute QY increased from 2.95% to 35.39%). The fluorescence lifetime was extended from 6.17 ns to 33.20 ns, and green fluorescence and longwave emission at 732 nm appeared in the modified biomass. This illustrates that different biomass carbon sources should be selected with appropriate nitrogen dopants.

Unlike nitrogen atoms, the addition of sulfur atoms regulates the original electron localization density of BCQDs, and the S/O on the surface has a high affinity for certain ions, which results in the formation of complexes to achieve fluorescence quenching.⁶⁰ Hu *et al.*¹¹¹ prepared nitrogen and sulfur co-doped BCQDs with a QY of 14.8% using green tea leaves as the carbon source, and pointed out that the enhancement of QY is mainly due to the stable combination of nitrogen atoms and carbon atoms, while sulfur atoms can provide a higher density of emission trap states, thereby changing the band gap of BCQDs. Yang *et al.*¹¹² used lignin as the raw material and concentrated sulfuric acid as the acidolysis agent and dopant to prepare sulfur-doped BCQDs *via* a hydrothermal method, and increased the QY of BCQDs from 3% to 13.5% by adjusting the amount of concentrated sulfuric acid added. When preparing sulfur-doped BCQDs from durian pulp *via* a hydrothermal method, Wang *et al.*⁶³ found that the incorporation of S with low electronegativity into the lattice enhanced the charge injection effect, thus exhibiting an ultra-high QY of 79%.

Heteroatom-doped BCQDs have good prospects for biosensing because they compensate for the poor fluorescence performance and single chemical structure of nondoped BCQDs. The addition of heteroatoms enriches the groups on the surface of BCQDs, which is conducive to the enhancement of interactions with heavy metal ions and thus improves the selectivity and sensitivity to heavy metal ions. Moreover, the addition of heteroatoms changes the energy level structure of BCQDs, which can regulate the fluorescence characteristics of BCQDs and broaden the application scope of BCQDs. Currently, the emission wavelengths of the prepared BCQDs are mainly short (blue-green light), and there are relatively few BCQDs with infrared/near-infrared emission, which greatly limits the application of doped BCQDs in practical detection. It is necessary to explore synthesis methods combining heteroatom doping with solvent conditioning and domain-limited growth and purification methods to develop additional BCQDs with red fluorescence emission and study their luminescence mechanism.

Application of BCQDs

BCQDs have the advantages of tunable optical properties, good biocompatibility, and high photostability and are extensively applied in biosensing.¹¹³

Array sensing

The surface of BCQDs contains numerous active functional groups, which can be altered by modifying the raw materials, synthesis techniques, or reaction parameters. These functional groups give BCQDs unique nonspecific interactions with a variety of target substances: the same kind of CQDs and different targets will produce different fluorescence response signals. Different BCQDs and the same target to be tested will also produce different fluorescence response signals, which can be distinguished by principal component analysis or linear discriminant analysis, thus identifying different targets to be tested. Therefore, BCQDs have become an excellent candidate material for the receptor unit of array sensors.

Fu *et al.*¹¹⁴ synthesized three types of BCQDs from three types of animal bones (pig, cow, and sheep bones) and constructed arrays of sensors for distinguishing the heavy metal ions Ag^+ , Cu^{2+} , Hg^{2+} , Fe^{3+} , and Pb^{2+} using these three types of BCQDs as sensing units (Fig. 8a). When the three types of BCQDs interacted with five different heavy metals, they produced different fluorescence responses. Fingerprinting showed that Fe^{3+} had the greatest effect on the bursting of the three types of BCQDs, whereas Ag^+ had the greatest effect on the bursting of the sheep bone BCQDs in the detection range of 40–4000 nM. Hierarchical clustering and linear discriminant analysis were employed to differentiate among Ag^+ , Cu^{2+} , Hg^{2+} , Fe^{3+} and Pb^{2+} . The precision was perfect at 100% for both single ions and combinations of two or three ions. BCQDs based on

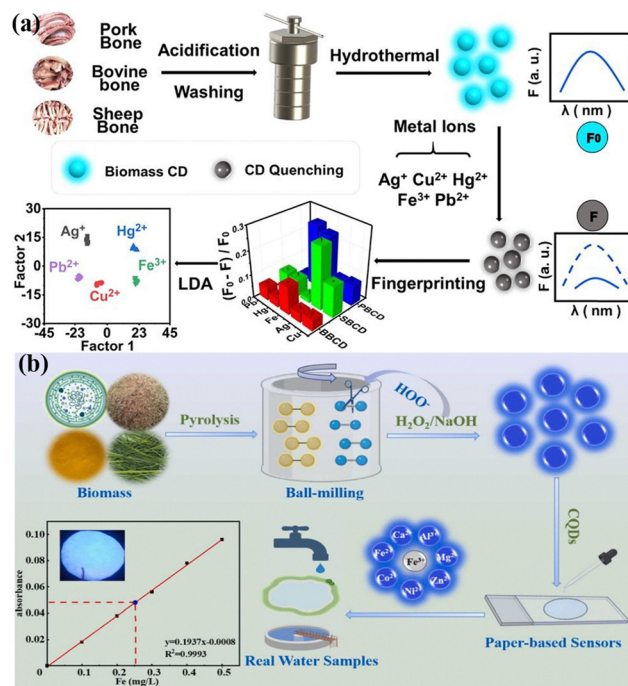


Fig. 8 (a) Preparation of bone biomass carbon dots and discrimination of five metal ions based on a multichannel BCQD array. Reproduced with permission from ref. 114. Copyright Elsevier, 2022. (b) Detection of Fe^{3+} by a BCQD paper sensor using cyanobacteria. Reproduced with permission from ref. 117. Copyright Elsevier, 2023.

Highlight

rowan walnut shells were prepared as molecularly imprinted polymers (CDs@MIPs) *via* a sol-gel process.¹¹⁵ The hollow spaces within the CDs@MIPs enabled the uncovered binding sites to selectively trap template molecules, significantly enhancing the specificity for 5-NDZs molecules. Different identifying materials that interact with 5-NDZs to varying degrees were used to differentiate between metronidazole, ornidazole, tinidazole, and tekridazole. Fingerprints were created based on the level of fluorescence variability, and the signals were examined using linear discriminant analysis. This array of fluorescent sensors can effectively detect these 5-NDZs across a broad range (20–5000 nM).

Paper-based sensing analysis

Due to the advantages of simplicity, speed, and visibility to the naked eye, paper-based sensors based on BCQDs have great application prospects in rapid visual detection applications. Based on tea seed hulls, Wang *et al.* developed a nitrogen-doped BCQD paper-based sensor for the visual sensing of glyphosate fluorescence.¹¹⁶ Under the optimal experimental conditions, glyphosate was detected in a two-stage linear pattern in the ranges of 0.1–0.6 μM and 0.6–1.6 μM , with a LOD of 0.075 μM . Next, the color recognition software for smartphones was used to detect the RGB values of glyphosate at various concentrations on the filter paper chip. The RGB values were in the range of 0.25–10.00 mM, with a LOD of 0.15 mM. The technique was used to analyze glyphosate-contaminated juice and flour samples, with recovery rates ranging from 87.60% to 112.69% for juice and 93.27% to 105.83% for flour. The excellent sensitivity and selectivity of cyanobacteria-based BCQDs for Fe^{3+} have been reported.¹¹⁷ Paper-based sensors made from BCQDs were created to easily and precisely detect Fe^{3+} in surface water, wastewater treatment plant effluent, and tap water (Fig. 8b). The R^2 of the blue-green algal BCQDs for Fe^{3+} detection reached 0.9956 when the Fe^{3+} concentration was between 0 and 60 μM . This study introduces a novel and dependable technique for producing BCQDs on a large scale.

Biological imaging

Bioimaging frequently relies on costly and harmful substances such as organic dyes and semiconductor quantum dots. There is a demand for fluorescent probes that are safer, more eco-friendly, and more affordable for bioimaging applications both in the lab and in living organisms. In these aspects, fluorescent probes made from biomass waste as starting materials may have higher potential.²⁶ In contrast to conventional organic fluorescent dyes and semiconductor quantum dots, BCQDs exhibit consistent optical characteristics and superior biocompatibility and are straightforward to synthesize and modify.³⁹ They are widely used in biosensors, biological imaging, nano-drug loading, and other fields. Notably, compared with most green or yellow fluorescent CQDs, red fluorescent CQDs sense interference in biological imaging and have unique advantages in the fields of cell and *in vivo* imaging.¹¹⁸ Recently, the development of high-performance near-infrared fluorescent CQDs as

contrast agents for cell imaging and *in vivo* imaging has become a research hotspot.

Red carbon dots were prepared from perilla, and four bacteria, namely, two Gram-positive bacteria (*Staphylococcus aureus* and *Enterococcus faecalis*) and two Gram-negative bacteria (*Escherichia coli* and *Salmonella*), were selected as representative models to investigate their period-imaging ability.¹¹⁹ Bacterial imaging experiments revealed that r-CNDs adhered more favorably to Gram-positive bacteria and away from Gram-negative bacteria than to blue and green bacteria. r-CNDs show potential as a bacterial visualizer for staining. L-Arginine-doped red/NIR-I fluorescent carbon dots (RA-CDs) were synthesized based on rhubarbic acid, a biologically active compound in traditional Chinese medicine.¹²⁰ RA-CD retained some of the functional groups of the active precursor, increased the solubility of rhubarbic acid, and emitted red/NIR-I light for bioimaging. *In vitro* experiments have shown that RA-CD scavenges

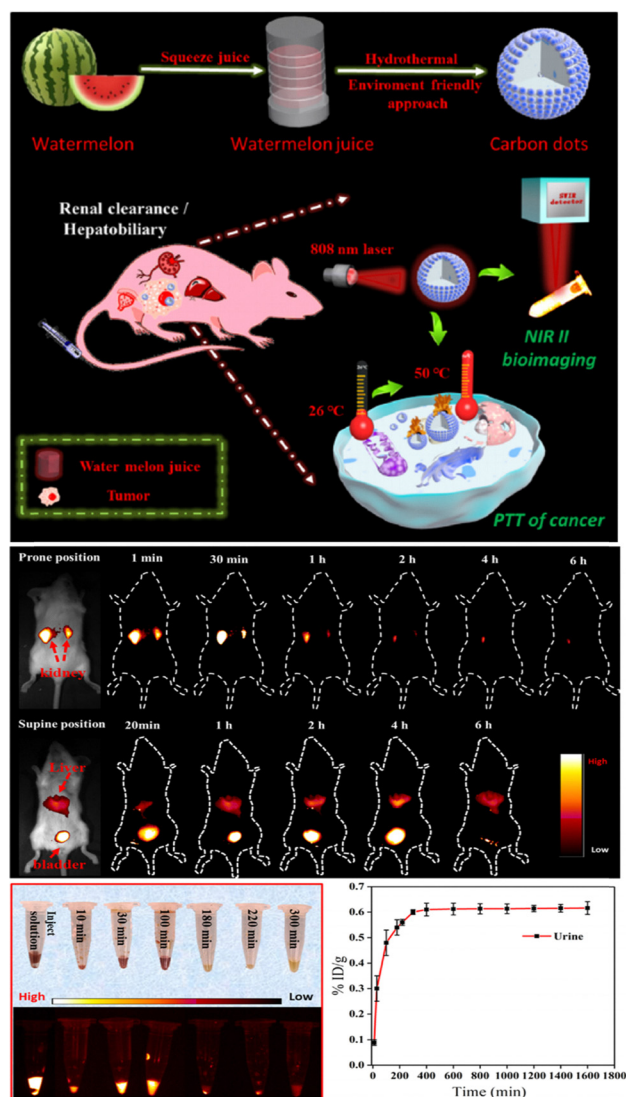


Fig. 9 Synthesis of NIR-II-emitting BCQDs for rapid renal clearance NIR-II bioimaging. Reproduced with permission from ref. 121. Copyright American Chemical Society, 2019.

excess reactive oxygen species (ROS), protects cells from oxidative stress, and enables fluorescence imaging of the inflamed colon. Li *et al.*¹²¹ synthesized red fluorescent BCQDs for *in vivo* optical imaging contrast agent emission in the near-infrared II region from watermelon juice and used them for *in vivo* imaging in mice (Fig. 9). The results showed that under 808 nm laser excitation, the BCQDs produced red fluorescence emission peaks at 900–1200 nm, which could be used for *in vivo* optical imaging in the NIR II region in mice. Notably, nearly 65% of the CQDs were excreted in the urine of the mice within 6 h, indicating that the kidneys could rapidly remove the CQDs from the body. In addition, the CQDs also exhibited a high photothermal efficiency (30.6%) under 808 nm light excitation, overcoming the limitations of *in vivo* high-sensitivity optical imaging that cannot be achieved by conventional visible light-emitting BCQDs and making the BCQDs more competitive in the field of optical imaging.

Conclusion and outlook

BCQDs provide significant advantages in biosensing, including low cytotoxicity, high fluorescence stability, and excellent biocompatibility. Compared with CQDs derived from chemical carbon sources, BCQDs use abundant and often waste biomass feedstocks, providing a sustainable and cost-effective alternative and enabling value-added utilization of waste. Despite substantial progress in research, key challenges hinder their wider application translation, particularly in biosensing and bioimaging.

First is the complexity of their preparation processes and yield bottlenecks. The preparation of BCQDs typically involves multiple steps with numerous influencing factors, and their synthesis and performance regulation are often separate. Current studies mostly focus on regulating BCQDs' performance through raw material pretreatment or cumbersome post-treatment, resulting in complex, time-consuming overall processes and generally low production yields. Thus, developing simplified integrated preparation processes to achieve the integration of BCQD synthesis, *in situ* regulation, and efficient purification, while simultaneously improving production yield and optical performance, is crucial for large-scale production and cost reduction. Second, enhanced optical performance in bioimaging needs further improvement. Although BCQDs have advantages in deep tissue imaging due to good tissue penetration depth and low photodamage, their low QY in aqueous solutions severely limits sensitivity in cellular and *in vivo* applications. Enhancing their QY under physiological conditions *via* advanced surface engineering and novel doping strategies is key to meeting clinical diagnostic needs. Third, there is a need to develop doped BCQD composites with reusability, portability, and enhanced functionalities such as magnetism and catalysis. Integrating them into point-of-care diagnostic devices or wearable sensors is central to achieving practical applications. Moreover, translating BCQDs from research to clinical and commercial reality requires rigorous

evaluation of their long-term biocompatibility, *in vivo* distribution, pharmacokinetics, and clearance properties to meet regulatory standards. In specific clinical applications such as intraoperative imaging and targeted therapy monitoring, demonstrating their significant advantages over existing reagents in terms of safety, efficacy, and cost-effectiveness is critical.

In summary, focusing on material optimization and large-scale production to overcome current technical bottlenecks, while advancing clinical translation and marketing purposes, is vital to fully unlocking the potential of BCQDs as transformative tools in biosensing and bioimaging fields.

Author contributions

Wen He: investigation, conceptualization, and writing – original draft; Deliang Zhang and Yan Gao: data curation and funding acquisition; Dongrun Li and Xing Gao: preparing figures; Hongyu Mou and Jibin Song: conceptualization and reviewing the paper.

Conflicts of interest

There are no conflicts to declare.

Data availability

No primary research results, software or code have been included and no new data were generated or analysed as part of this review.

Acknowledgements

This work was supported by the Research Program of the National key research and development plan (No. 2023YFB3810002), Beijing Outstanding Young Scientist Program (JWZQ20240101010), the National Natural Science Foundation of China (No. U21A20377, U22A20348), Qilu Institute of Technology (No. QIT23TP018), and the Natural Science Foundation of Shandong Province (ZR2022QB073).

Notes and references

- 1 H. B. Sousa, C. S. Martins and J. A. Prior, *Nanomaterials*, 2021, **11**, 611.
- 2 (a) L. J. Desmond, A. N. Phan and P. Gentile, *Environ. Sci. Nano*, 2021, **8**, 848–862; (b) D. Zhang, D. Chao, C. Yu, Q. Zhu, S. Zhou, L. Tian and L. Zhou, *J. Phys. Chem. Lett.*, 2021, **12**, 8939–8946; (c) V. Manikandan and N. Y. Lee, *Environ. Res.*, 2022, **212**, 113283.
- 3 (a) W. Z. Yu, Q. Li, L. Q. He and X. L. Xiao, *Anal. Methods*, 2023, **15**, 944–950; (b) M. Pourmadadi, E. Rahmani, M. Rajabzadeh-Khosroshahi, A. Samadi, R. Behzadmehr and A. Rahdar, *J. Drug Delivery Sci. Technol.*, 2023, **80**, 104156.
- 4 T. C. Wareing, P. Gentile and A. N. Phan, *ACS Nano*, 2021, **15**, 15471–15501.
- 5 H. Xu, W. H. Zhan, M. J. Wan, X. D. Bao, L. Tang and X. Guan, *Ind. Crops Prod.*, 2025, **227**, 120775.
- 6 T. Chopra, S. Sasan, L. Devi, R. Parkesh and K. K. Kapoor, *Coord. Chem. Rev.*, 2022, **470**, 214704.
- 7 K. M. Low, X. Lin, H. Li and S. F. Y. Wu, *Polymers*, 2024, **16**, 652.

- 8 T. He, Q. Tang, Q. Ren, Y. Liu, G. He, Y. Pan, Z. Wang, P. Huang and J. Lin, *ACS Nano*, 2024, **18**, 5434–5445.
- 9 N. Zhang, L. Zhao, M. He, P. Luo and L. Tan, *Spectrochim. Acta, Part A*, 2023, **284**, 121771.
- 10 R. C. Timson, A. Khan, B. Uygur, M. Saad, H. W. Yeh, N. L. DelGaudio and K. Birsoy, *J. Biol. Chem.*, 2024, **300**, 105645.
- 11 (a) Z. Yan, Y. Cai, J. Zhang and Y. Zhao, *Measurement*, 2022, **187**, 110355; (b) R. AbhijnaKrishna and S. Velmathi, *Coord. Chem. Rev.*, 2022, **459**, 214401.
- 12 T. Zhang, J. Zhou, H. Li, J. Ma, X. Wang, H. Shi and Y. Guo, *Green Chem.*, 2023, **25**, 1406–1416.
- 13 N. Chaudhary, P. K. Gupta, S. Eremin and P. R. Solanki, *J. Environ. Chem. Eng.*, 2020, **8**, 103720.
- 14 F. G. Torres, K. N. Gonzales, O. P. Troncoso and V. S. Cañedo, *Mar. Drugs*, 2023, **21**, 338.
- 15 P. E. Cardoso-Ávila, J. L. Pichardo-Molina, M. Vázquez-Olmos and E. González-Aguíñaga, *Mater. Lett.*, 2024, **358**, 135880.
- 16 J. Goswami, S. S. Rohman, A. K. Guha, P. Basyach, K. Sonowal, S. P. Borah, L. Saikia and P. Hazarika, *Mater. Chem. Phys.*, 2022, **286**, 126133.
- 17 M. Rani, U. Shanker, B. S. Kaith and M. Sillanpää, *Inorg. Chem. Commun.*, 2024, **159**, 111878.
- 18 J. Wang, Y. Sun, P. Wang, Z. Sun, Y. Wang, M. Gao and X. Wang, *Anal. Chim. Acta*, 2024, **1289**, 342182.
- 19 I. Prgommet, N. Pascual-Seva, M. C. Morais, A. Aires, D. Barreales, A. C. Ribeiro and B. Gonçalves, *Sci. Hortic.*, 2020, **261**, 108990.
- 20 W. He, S. F. Lim, R. Baini, Y. P. Qu and X. J. Li, *Anal. Lett.*, 2025, **58**, 228–241.
- 21 Z. G. Ye, Y. H. Zhang, G. X. Li and B. X. Li, *Anal. Lett.*, 2020, **53**, 2841–2853.
- 22 K. W. Kim, T. Y. Choi, Y. M. Kwon and J. Y. H. Kim, *Electron. J. Biotechnol.*, 2020, **47**, 36–42.
- 23 C. Xu, J. Kang, Y. Zhao, L. Zhu, J. Zhang, B. Wei and H. Wang, *New J. Chem.*, 2023, **47**, 3159–3166.
- 24 W. A. Amer, A. F. Rehab, M. E. Abdelghafar, N. L. Torad, A. S. Atlam and M. M. Ayad, *Carbon*, 2021, **179**, 159–171.
- 25 G. Chellamy, S. K. Arumugam, S. Govindaraju and K. Yun, *Chemosphere*, 2022, **287**, 131915.
- 26 H. Ren, Y. Yuan, A. Labidi, Q. Dong, K. Zhang, E. Lichtfouse and C. Wang, *Chin. Chem. Lett.*, 2023, **34**, 107998.
- 27 D. B. Gunjal, Y. M. Gurav, A. H. Gore and G. B. Kolekar, *Opt. Mater.*, 2019, **98**, 109484.
- 28 H. C. Liu, L. Ding, L. G. Chen, Y. H. Chen, T. Y. Zhou, H. Y. Li, Y. Xu, L. Zhao and N. Huang, *J. Ind. Eng. Chem.*, 2019, **69**, 455–463.
- 29 J. C. Fei and S. W. Sun, *Biomass Convers. Biorefin.*, 2023, **14**, 1–9.
- 30 K. Kasinathan, S. Samayanan, K. Marimuthu and J. H. Yim, *Appl. Surf. Sci.*, 2022, **601**, 154266.
- 31 J. S. Britto, X. Guan, T. K. A. Tran, Z. Lei, R. Bahadur, V. Patel and A. Vinu, *Small Sci.*, 2024, **4**, 2300221.
- 32 C. Pan, J. He, J. Zhu, S. Li, W. Li, W. Yang and W. Li, *ACS Appl. Nano Mater.*, 2024, **7**, 2515–2528.
- 33 (a) A. Padmapriya, P. Thiagarajan, M. Devendiran, R. A. Kalaivani and A. M. Shanmugharaj, *J. Electroanal. Chem.*, 2023, **943**, 117609; (b) S. N. Qu, D. Zhou, D. Li, W. Y. Ji, P. T. Jing, D. Han, L. Liu, H. B. Zeng and D. Z. Shen, *Adv. Mater.*, 2016, **28**, 3516–3521.
- 34 H. Wang, P. Sun, S. Cong, J. Wu, L. Gao, Y. Wang and G. Zou, *Nanoscale Res. Lett.*, 2016, **11**, 1–6.
- 35 Z. Ye, X. Lin, N. Wang, J. Zhou, M. Zhu, H. Qin and X. Peng, *Nat. Commun.*, 2021, **12**, 4283.
- 36 F. Qin, J. Bai, Y. Zhu, P. He, X. Wang, S. Wu and L. Ren, *Phys. Chem. Chem. Phys.*, 2023, **25**, 2762–2769.
- 37 (a) Y. M. Xian and K. Li, *Adv. Mater.*, 2022, **34**, 2201031; (b) H. Sun, S. Xu, Z. Chen, F. Liu, S. Zong, Z. Wang and C. Wang, *Mater. Res. Bull.*, 2023, **159**, 112092.
- 38 (a) F. Yuan, T. Yuan, L. Sui, Z. Wang, Z. Xi, Y. Li and S. Yang, *Nat. Commun.*, 2018, **9**, 2249; (b) F. Yuan, Y. K. Wang, G. Sharma, Y. Dong, X. Zheng, P. Li and E. H. Sargent, *Nat. Photonics*, 2020, **14**, 171–176.
- 39 J. Liu, Y. Geng, D. Li, H. Yao, Z. Huo, Y. Li and B. Yang, *Adv. Mater.*, 2020, **32**, 1906641.
- 40 (a) Y. Liu, C. Wu, Y. Niu, T. Meng and J. He, *J. Phys. Chem. Lett.*, 2024, **15**, 1584–1589; (b) Y. Li, L. Chen, S. Yang, G. Wei, X. Ren, A. Xu and G. Ding, *Adv. Mater.*, 2024, **36**, 2313639.
- 41 Y. S. Liu, H. Yang, T. Huang, L. Niu and S. Liu, *Nano Today*, 2024, **56**, 102257.
- 42 X. Wu, C. Ma, J. Liu, Y. Liu, S. Luo, M. Xu and S. Liu, *ACS Sustainable Chem. Eng.*, 2019, **7**, 18801–18809.
- 43 X. Zhang, H. Guo, C. Chen, B. Quan, Z. Zeng, J. Xu and L. Wang, *Appl. Mater. Today*, 2023, **30**, 101706.
- 44 J. Shi, Y. Zhou, J. Ning, G. Hu, Q. Zhang, Y. Hou and Y. Zhou, *Spectrochim. Acta, Part A*, 2022, **281**, 121597.
- 45 Z. He, M. Yuen, C. Zhang, J. Zhang, Z. Wang, C. Yue and K. Zhang, *J. Mater. Chem. C*, 2024, **12**, 6333–6340.
- 46 (a) Y. Lou, X. Y. Hao, L. Liao and Z. Li, *Nano Sel.*, 2021, **2**, 1117–1145; (b) S. Durrani, J. Zhang, Mukramin, H. Wang, Z. Wang, L. U. Khan, F. Zhang, F. Durrani, F. G. Wu and F. Lin, *ACS Appl. Nano Mater.*, 2023, **6**, 76–85.
- 47 Y. N. Mao, J. Wang, Y. H. Gao and X. L. Luo, *Chin. J. Anal. Chem.*, 2021, **49**, 1076–1088.
- 48 B. Zhang, C. Y. Liu and Y. Liu, *Eur. J. Inorg. Chem.*, 2010, 4411–4414.
- 49 S. Zhao, M. Lan, X. Zhu, H. Xue, T. W. Ng, X. Meng and W. Zhang, *ACS Appl. Mater. Interfaces*, 2015, **7**, 17054–17060.
- 50 H. Ding, Y. Ji, J. S. Wei, Q. Y. Gao, Z. Y. Zhou and H. M. Xiong, *J. Mater. Chem. B*, 2017, **5**, 5272–5277.
- 51 X. J. Wei, L. Li, J. L. Liu, L. D. Yu, H. B. Li, F. Cheng, X. T. Yi, J. M. He and B. S. Li, *ACS Appl. Mater. Interfaces*, 2019, **11**, 9832–9840.
- 52 M. He, X. Fu, G. Du, H. Li, P. P. Zhao and X. Liu, *Packag. Technol. Sci.*, 2023, **36**, 465–472.
- 53 L. Feng, S. Zheng, X. Ma, H. Zhu, Z. Hu and Y. Sun, *Microchem. J.*, 2024, **199**, 110003.
- 54 Y. Liu, Y. Tang, Q. Xu, Y. Cao, J. Wei, Z. Liang and C. Guo, *J. Lumin.*, 2024, **271**, 120583.
- 55 S. Patra, M. Singh, S. Subudhi, M. Mandal, A. K. Nayak, B. B. Sahu and P. Mahanandia, *J. Photochem. Photobiol. A*, 2023, **442**, 114779.
- 56 B. K. John, J. Mathew, K. Sreekanth and B. Mathew, *Mater. Today Sustainability*, 2024, **24**, 100715.
- 57 D. Rodriguez-Padron, M. Algarra, L. A. Tarelho, J. Frade, A. Franco, G. de Miguel and R. Luque, *ACS Sustainable Chem. Eng.*, 2018, **6**, 7200–7205.
- 58 R. E. Kannouma, A. H. Kamal, M. A. Hammad and F. R. Mansour, *Microchem. J.*, 2024, **200**, 110397.
- 59 M. Nazar, M. Hasan, B. Wirjosentono, B. A. Gani and C. E. Nada, *ACS Omega*, 2024, **9**, 20571–20581.
- 60 A. Yadav, R. Yadav, V. Lahariya and A. K. Singh, *Res. Chem. Intermed.*, 2024, **50**, 1873–1893.
- 61 N. A. Qandeel, A. A. El-Masry, M. Eid, M. A. Moustafa and R. El-Shaheny, *Anal. Chim. Acta*, 2023, **1237**, 340592.
- 62 B. Thangaraj, P. R. Solomon, S. Chuangchote, N. Wongyao and W. Surareungchai, *ChemBioEng Rev.*, 2021, **8**, 265–301.
- 63 G. Wang, Q. L. Guo, D. Chen, Z. D. Liu, X. H. Zheng, A. L. Xu, S. W. Yang and G. Q. Ding, *ACS Appl. Mater. Interfaces*, 2018, **10**, 5750–5759.
- 64 Y. Wu, Y. D. Li, X. Q. Pan, C. F. Hu, J. L. Zhuang, X. J. Zhang, B. F. Lei and Y. L. Liu, *New J. Chem.*, 2021, **45**, 5484–5490.
- 65 Z. Deng, C. Liu, Y. Jin, J. Pu, B. Wang and J. Chen, *Analyst*, 2019, **144**, 4569–4574.
- 66 C. Xu, X. Xiao, C. Cai, Q. Cheng, L. Zhu, J. Zhang, B. Wei and H. Wang, *Environ. Sci. Pollut. Res.*, 2023, **30**, 57301–57311.
- 67 S. Gulati, A. Baul, A. Amar, R. Wadhwa, S. Kumar and R. S. Varma, *Nanomaterials*, 2023, **13**, 554.
- 68 O. Kozak, M. Sudolska, G. Pramanik, P. Cigler, M. Otyepka and R. Zboril, *Chem. Mater.*, 2016, **28**, 4085–4128.
- 69 X. Yan, B. Li and L. S. Li, *Acc. Chem. Res.*, 2013, **46**, 2254–2262.
- 70 F. Yuan, Z. Wang, X. Li, Y. Li, Z. A. Tan, L. Fan and S. Yang, *Adv. Mater.*, 2017, **29**, 1604436.
- 71 K. Jiang, S. Sun, L. Zhang, Y. Lu, A. Wu, C. Cai and H. Lin, *Angew. Chem.*, 2015, **127**, 5450–5453.
- 72 H. Li, X. He, Z. Kang, H. Huang, Y. Liu, J. Liu and S. T. Lee, *Angew. Chem., Int. Ed.*, 2010, **49**, 4430–4434.
- 73 J. Peng, W. Gao, B. K. Gupta, Z. Liu, R. Romero-Aburto, L. Ge and P. M. Ajayan, *Nano Lett.*, 2012, **12**, 844–849.
- 74 (a) P. M. Gharat, J. M. Chethodil, A. P. Prastava, P. K. Praseetha, H. Pal and S. D. Choudhury, *Photochem. Photobiol. Sci.*, 2019, **18**, 110–119; (b) D. Shen, Y. Long, J. Wang, Y. Yu, J. Pi, L. Yang and H. Zheng, *Nanoscale*, 2019, **11**, 5998–6003.
- 75 L. Bao, Z. L. Zhang, Z. Q. Tian, L. Zhang, C. Liu, Y. Lin and D. W. Pang, *Adv. Mater.*, 2011, **23**, 5801–5806.
- 76 H. Ding, S. B. Yu, J. S. Wei and H. M. Xiong, *ACS Nano*, 2016, **10**, 484–491.

- 77 Y. Zhang, R. Yuan, M. He, G. Hu, J. Jiang, T. Xu and X. Liang, *Nanoscale*, 2017, **9**, 17849–17858.
- 78 Y. Song, S. Zhu, S. Zhang, Y. Fu, L. Wang, X. Zhao and B. Yang, *J. Mater. Chem. C*, 2015, **3**, 5976–5984.
- 79 L. Cao, M. H. Zan, F. M. Chen, X. Y. Kou, Y. L. Liu, P. Y. Wang, Q. Mei, Z. Hou, W. F. Dong and L. Li, *Carbon*, 2022, **194**, 42–51.
- 80 P. F. Li, S. S. Xue, L. Sun, X. B. Ma, W. N. Liu, L. An, Y. C. Liu, D. Qu and Z. C. Sun, *Small*, 2024, **20**, 2310563.
- 81 Y. Z. Liu, P. F. Li and Z. C. Sun, *Chem. Res. Chin. Univ.*, 2025, **46**, 20250103.
- 82 X. Sun and Y. Lei, *Trends Anal. Chem.*, 2017, **88**, 106–128.
- 83 L. Wang, Y. Ji, Y. Chen, S. Zheng, F. Wang and C. Li, *Trends Anal. Chem.*, 2024, **180**, 117962.
- 84 S. Hijazi, A. S. Ganie, M. M. Rahman and W. A. Shah, *Environ. Sci.:Nano*, 2023, **10**, 3281–3294.
- 85 X. J. Jiang, Y. Ma, Y. Zhou, R. D. Xiao, Y. J. Meng, B. T. Xie and D. H. Zhao, *Spectrochim. Acta, Part A*, 2024, **316**, 124305.
- 86 Q. Zhang, S. He, K. Zheng, L. Zhang, L. Lin, F. Chen and B. Li, *Inorg. Chem. Commun.*, 2022, **146**, 110034.
- 87 F. Zu, F. Yan, Z. Bai, J. Xu, Y. Wang, Y. Huang and X. Zhou, *Microchim. Acta*, 2017, **184**, 1899–1914.
- 88 W. Li, K. Luo, M. Lv and Y. Wen, *J. Nanopart. Res.*, 2024, **26**, 70.
- 89 Z. G. Ge, H. Y. Du, B. Tang and J. Deng, *J. Fluoresc.*, 2025, **35**, 3019–3032.
- 90 Y. Z. Fan, Y. Zhang, N. Li, S. G. Liu, T. Liu, N. B. Li and H. Q. Luo, *Sens. Actuators, B*, 2017, **240**, 949–955.
- 91 A. Hemmati, H. Emadi and S. R. Nabavi, *ACS Omega*, 2023, **8**, 20987–20999.
- 92 X. X. Ma, M. H. Geng, X. Y. Cheng, T. S. Zhang, Z. L. Li and K. Zhao, *Phys. Chem. Chem. Phys.*, 2024, **26**, 6008–6021.
- 93 P. Murugesan, N. Libiya, J. A. Moses and C. Anandharamakrishnan, *Carbon Lett.*, 2023, **33**, 2335–2348.
- 94 Y. Zhu, X. Deng, J. Chen, Z. Hu and F. Wu, *Food Chem.*, 2023, **429**, 136957.
- 95 H. Ding, R. Zhao, Z. H. Zhang, J. J. Yang, Z. Wang, L. L. Xiao and H. M. Xiong, *Chem. Eng. J.*, 2023, **476**, 146405.
- 96 Y. Q. Han, J. X. Ni, X. L. Huang, Y. D. Li, G. Q. Jiang and S. Y. Han, *Chem. Ind. For. Prod.*, 2021, **41**, 58–64.
- 97 A. Sciortino, A. Panniello, G. Minervini, N. Mauro, G. Giammona, G. Buscarino and F. Messina, *Mater. Res. Bull.*, 2022, **149**, 111746.
- 98 T. Wang, X. Q. Liu, Q. Y. Men, C. C. Ma, Y. Liu, W. Ma, Z. Liu, M. B. Wei, C. X. Li and Y. S. Yan, *Chin. J. Catal.*, 2019, **40**, 886–894.
- 99 K. Fang, Y. Wu, J. Yang, N. Wang, K. Mo, C. Zeng and B. Deng, *Spectrochim. Acta, Part A*, 2024, **306**, 123616.
- 100 Y. Dai, W. Xu, J. Hong, Y. Zheng, H. Fan, J. Zhang and J. Hong, *Biosens. Bioelectron.*, 2023, **238**, 115559.
- 101 Z. Zhan, H. Mao, M. Xue, G. Han, G. Zhou and Y. Zhang, *Methods Appl. Fluoresc.*, 2023, **12**, 015004.
- 102 A. Prakash, S. Yadav, U. Yadav, P. S. Saxena and A. Srivastava, *Bull. Mater. Sci.*, 2023, **46**, 7.
- 103 A. S. Sethulekshmi, A. Aparna, P. Parvathi, R. Pathak, V. D. Punetha, M. Selvaraj and A. Saritha, *Chem. Eng. J.*, 2025, **514**, 163262.
- 104 Q. Huang, Q. Li, Y. Chen, L. Tong, X. Lin, J. Zhu and Q. Tong, *Sens. Actuators, B*, 2018, **276**, 82–88.
- 105 J. Yu, N. Song, Y. K. Zhang, S. X. Zhong, A. J. Wang and J. Chen, *Sens. Actuators, B*, 2015, **214**, 29–35.
- 106 W. Liu, H. Diao, H. Chang, H. Wang, T. Li and W. Wei, *Sens. Actuators, B*, 2017, **241**, 190–198.
- 107 X. Niu, G. Liu, L. Li, Z. Fu, H. Xu and F. Cui, *RSC Adv.*, 2015, **5**, 95223–95229.
- 108 R. C. Wang, J. T. Lu and Y. C. Lin, *J. Alloys Compd.*, 2020, **813**, 152201.
- 109 Z. Wang, Q. H. Liu, J. P. Leng, H. Y. Liu, Y. X. Zhang, C. D. Wang, W. Q. An, C. N. Bao and H. Lei, *J. Saudi Chem. Soc.*, 2021, **25**, 101373.
- 110 Y. Liu, C. Yong, B. Tong, Y. Li, N. Wang and Y. Lei, *Opt. Mater.*, 2022, **134**, 113144.
- 111 Z. Hu, X. Jiao and L. Xu, *Microchem. J.*, 2020, **154**, 104588.
- 112 X. Yang, Y. Guo, S. Liang, S. Y. Hou, T. T. Chu, J. L. Ma, X. H. Chen, J. H. Zhou and R. C. Sun, *J. Mater. Chem. B*, 2020, **8**, 10788–10796.
- 113 X. Guan, Z. Li, X. Geng, Z. Lei, A. Karakoti, T. Wu and A. Vinu, *Small*, 2023, **19**, 2207181.
- 114 L. Fu, T. Liu, F. Yang, M. Wu, C. Yin, L. Chen and N. Niu, *J. Photochem. Photobiol., A*, 2022, **424**, 113638.
- 115 Q. Sun, L. Fu, C. Yin, M. Wu, H. Liu, N. Niu and L. Chen, *Sens. Actuators, B*, 2022, **373**, 132716.
- 116 X. Wang, Y. Lv, X. Kong, Z. Ding, X. Cheng, Z. Liu and G.-C. Han, *New J. Chem.*, 2023, **47**, 10696–10705.
- 117 H. C. Hao, S. Chen, Z. X. Tan and H. Jiang, *J. Environ. Chem. Eng.*, 2023, **11**, 111406.
- 118 J. Li, S. Yang, Z. Liu, G. Wang, P. He, W. Wei and X. Fan, *Adv. Mater.*, 2021, **33**, 2005096.
- 119 W. Zhao, Y. Wang, K. Liu, R. Zhou and C. Shan, *Chin. Chem. Lett.*, 2022, **33**, 798–802.
- 120 J. S. Xia, J. Y. Wang, F. Y. Liu, Z. Q. Chen, C. M. Chen, X. S. Cheng, Y. Chao, Y. Wang and T. Deng, *Adv. Healthcare Mater.*, 2024, **13**, 2304674.
- 121 Y. Li, G. Bai, S. Zeng and J. Hao, *ACS Appl. Mater. Interfaces*, 2019, **11**, 4737–4744.